2.6.7 細胞培養士の認定制度の確立

品質のよい幹細胞を維持するためには，高い培養技術を有する技術者が必要である．技術者を育てるには，培養に熟練した指導者が必要である．しかし，幹細胞を培養するためにはまず，基本的な培養技術・知識を身につけておく必要がある．日本組織培養学会は，細胞培養における基盤的技術の講習会を開催し，細胞培養士の資格を授与するとともに，指導者認定制度も立ち上げている（図 2.6.3）．ヒト幹細胞の実用化のためには，細胞培養学に基づいた基本的な培養技術の標準化を図る必要がある．

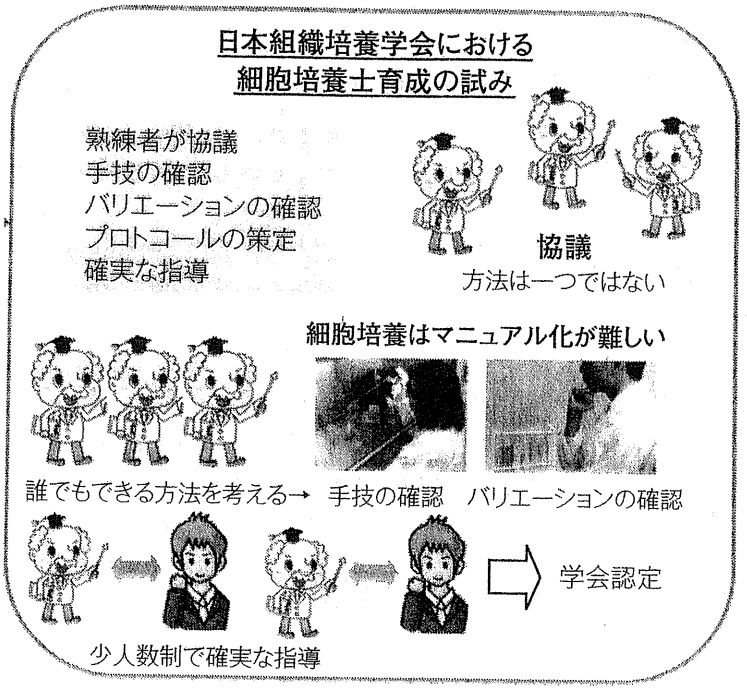

図 2.6.3 細胞培養士の認定制度

2.6.8 おわりに

現時点においては，ヒト ES/iPS 細胞はその樹立の方法や培養条件のみならず，培養技術が研究室により異なるために，結果が追試できないことも多い．実用化においては，ヒト ES/iPS 細胞の細胞特性を深く理解し，培養技術・品

質評価を定義することで世界中どこでも誰が行っても同じように細胞を調製できることが重要である．国内外において2012年現在，ヒト多能性幹細胞の臨床試験が開始されつつある．実用化に向けて，ロット差のない組成の明らかな培地を用い，培養工程の正確な記録を行うことにより，培養技術の標準化を進めていく必要がある．

参考文献

1) Adewumi, O., et al. (2007). Characterization of human embryonic stem cell lines by the International Stem Cell Initiative. *Nat Biotechnol.*
2) Furue, M.K. (2008). Standardization of human embryonic stem (ES) cell and induced pulripoent stem (iPS) cell research in Japan. *Tissue Culture Research Communications* **27**:139–147.
3) Furue, M.K. (2009). Standardization of human embryonic stem (ES) cell and induced pulripoent stem (iPS) cell research in Japan: How to detect differentiation potency of human ES/iPS cells. *Tissue Culture Research Communications* **28**:129-133.
4) Amps, K., et al. (2011). Screening ethnically diverse human embryonic stem cells identifies a chromosome 20 minimal amplicon conferring growth advantage. *Nat Biotechnol* **29**(12):1132–1144.
5) Draper, J.S., et al. (2004). Recurrent gain of chromosomes 17q and 12 in cultured human embryonic stem cells. *Nat Biotechnol* **22**(1):53–54.
6) Baker, D.E., et al.(2007). Adaptation to culture of human embryonic stem cells and oncogenesis in vivo. *Nat Biotechnol* **25**(2):207–215.
7) Ramos-Mejia, V., et al. (2010). iPSC lines that do not silence the expression of the ectopic reprogramming factors may display enhanced propensity to genomic instability. *Cell Res* **20**(10):1092–1095.
8) Kinoshita, T., et al. (2011). Ataxia-telangiectasia mutated (ATM) deficiency decreases reprogramming efficiency and leads to genomic instability in iPS cells. *Biochem Biophys Res Commun* **407**(2):321–326.
9) Olariu, V., et al. (2010). Modeling the evolution of culture-adapted human embryonic stem cells. *Stem Cell Res* **4**(1):50–56.
10) Hirata, M., et al. (2011). Quality control for human embryonic stem (ES) cell and induced pulripoent stem (iPS) cells on the bench. *Tissue Culture Research Communications* **30**:145–157.
11) Amit, M., et al. (2004). Feeder layer- and serum-free culture of human embryonic stem cells. *Biol Reprod* **70**(3):837–845.

12) Hayashi, Y., et al. (2010). Reduction of N-glycolylneuraminic acid in human induced pluripotent stem cells generated or cultured under feeder- and serum-free defined conditions. *PLoS One* **5**(11): e14099.
13) Barnes, D. and G. Sato (1980) .Serum-free cell culture: a unifying approach. *Cell* **22**(3):649–655.
14) Sato, G. (1975). Biochemical Actions of Hormones. *Academic* pp.391–396.
15) Hayashi, I. and G.H. Sato. (1976). Replacement of serum by hormones permits growth of cells in a defined medium. *Nature* **259**(5539):132–134.
16) Bottenstein, J., et al. (1979). The growth of cells in serum-free hormone-supplemented media. *Methods Enzymol* **58**:94–109.
17) Sato, J.D., Kawamoto, T., Okamoto,T. (1987).Cholesterol requirement of P3-X63-Ag8 and X63-Ag8.653 mouse myeloma cells for growth in vitro. *J Exp Med* **165**(6): 1761–1766.
18) Sato, J.D., et al. (2002). Specific cells and their requirements. in *Basic Cell Culture: A Practical Approach, 2nd Edn.*, J.M.Davis,Editor., Oxford University Press, England. pp.227–274.
19) Furue, M., et al. (1994). Primitive neuroectodermal tumor cell lines derived from a metastatic pediatric tumor. *In Vitro Cell Dev Biol Anim.* **30A**(12):813–816.
20) Furue, M. and S. Saito. (1998). Hepatocyte growth factor regulates activin bA mRNA in submandibular gland. *In Vitro Cell. Dev. Biol.* **34**:520–523.
21) Furue, M., et al. (1999). Effects of hepatocyte growth factor (HGF) and activin A on the morphogenesis of rat submandibular gland-derived epithelial cells in serum-free collagen gel culture. *In Vitro Cell Dev Biol Anim.* **35**(3):131–135.
22) Furue, M., M. Asashima, and R. Hata (2000). Establishment of RSMG-2 cell line derived from male rat submandibular gland in serum-free defined culture. *Tissue Culture Res. Commun* **19**:199–202.
23) Furue, M., et al. (2001). Activin A induces expression of rat Sel-1l mRNA, a negative regulator of notch signaling, in rat salivary gland-derived epithelial cells. *Biochem Biophys Res Commun* **282**(3):745–749.
24) Furue, M., et al. (2005). Leukemia inhibitory factor as an anti-apoptotic mitogen for pluripotent mouse embryonic stem cells in a serum-free medium without feeder cells. *In Vitro Cell Dev Biol Anim* **41**(1-2):19–28.
25) Brewer, G.J., et al. (1993). Optimized survival of hippocampal neurons in B 27-supplemented Neurobasal, a new serum-free medium combination. *J Neurosci Res* **35**(5):567–576.
26) Ludwig, T.E., et al. (2006). Derivation of human embryonic stem cells in defined conditions. *Nat Biotechnol* **24**(2):185–187.
27) Chen, G., et al. (2011). Chemically defined conditions for human iPSC derivation and culture. *Nat Methods* 8(5):424–429.

28) Furue, M.K., et al. (2008). Heparin promotes the growth of human embryonic stem cells in a defined serum-free medium. *Proc Natl Acad Sci U S A* **105**(36):13409–13414.

29) Na, J., Furue, M.K., Andrews, P.W. (2010). Inhibition of ERK 1/2 prevents neural and mesendodermal differentiation and promotes human embryonic stem cell self-renewal. *Stem Cell Res*

30) Vallier, L., Reynolds, D., Pedersen, R.A. (2004). Nodal inhibits differentiation of human embryonic stem cells along the neuroectodermal default pathway. *Dev Biol* **275**(2):403–421.

31) James, D., et al. (2005). TGFbeta/activin/nodal signaling is necessary for the maintenance of pluripotency in human embryonic stem cells. *Development* **132**(6): 1273–1282.

32) Pebay, A., et al. (2005). Essential roles of sphingosine-1-phosphate and platelet-derived growth factor in the maintenance of human embryonic stem cells. *Stem Cells* **23**(10):1541–1548.

33) Dvorak, P., Hampl, A. (2005). Basic fibroblast growth factor and its receptors in human embryonic stem cells. *Folia Histochem Cytobiol* **43**(4):203–208.

34) Avery, S., Inniss, K., Moore, H. (2006). The regulation of self-renewal in human embryonic stem cells. *Stem Cells Dev* **15**(5):729–740.

35) Ding, V.M., et al. (2011). Tyrosine phosphorylation profiling in FGF-2 stimulated human embryonic stem cells. *PLoS One* **6**(3): e17538.

36) Kawase, T., et al. (2009). Osteogenic activity of human periosteal sheets cultured on salmon collagen-coated ePTEE mesh. *Materials in medicine* **21**:731–739.

37) Lin, Z., et al. (2011). In vitro Evaluation of Natural Marine Sponge Collagen as a Scaffold for Bone Tissue Engineering International *Journal of Biological Sciences* **7**: 968–977.

38) 柳原佳奈，寺田聡，番戸博友，猪爪優子．(2011)．特願 2011-167665．幹細胞の分化誘導法．

39) Watanabe, K., et al. (2007). A ROCK inhibitor permits survival of dissociated human embryonic stem cells. *Nat Biotechnol* **25**(6):681–686.

40) Initiative, T.I.S.C.B. (2009). The International Stem Cell Banking Initiative. *Stem Cell Rev and Rep* **5**:301–314.

Biomaterials 34 (2013) 1781–1789

Contents lists available at SciVerse ScienceDirect

Biomaterials

journal homepage: www.elsevier.com/locate/biomaterials

3D spheroid culture of hESC/hiPSC-derived hepatocyte-like cells for drug toxicity testing

Kazuo Takayama [a,b], Kenji Kawabata [b,c], Yasuhito Nagamoto [a,b], Keisuke Kishimoto [a,b], Katsuhisa Tashiro [b], Fuminori Sakurai [a], Masashi Tachibana [a], Katsuhiro Kanda [d], Takao Hayakawa [e], Miho Kusuda Furue [f,g], Hiroyuki Mizuguchi [a,b,h,*]

[a] Laboratory of Biochemistry and Molecular Biology, Graduate School of Pharmaceutical Sciences, Osaka University, Osaka 565-0871, Japan
[b] Laboratory of Stem Cell Regulation, National Institute of Biomedical Innovation, Osaka 567-0085, Japan
[c] Laboratory of Biomedical Innovation, Graduate School of Pharmaceutical Sciences, Osaka University, Osaka 565-0871, Japan
[d] Pharma Business Project, Corporate Projects Center, Corporate Strategy Division, Hitachi High-Technologies Corporation, Ibaraki 312-8504, Japan
[e] Pharmaceutical Research and Technology Institute, Kinki University, Osaka 577-8502, Japan
[f] Laboratory of Embryonic Stem Cell Cultures, Department of Disease Bioresources Research, National Institute of Biomedical Innovation, Osaka 567-0085, Japan
[g] Department of Embryonic Stem Cell Research, Field of Stem Cell Reseach, Institute for Frontier Medical Sciences, Kyoto University, Kyoto 606-8507, Japan
[h] The Center for Advanced Medical Engineering and Informatics, Osaka University, Osaka 565-0871, Japan

ARTICLE INFO

Article history:
Received 11 September 2012
Accepted 20 November 2012
Available online 8 December 2012

Keywords:
Hepatocyte-like cell
Human ES cell
Human iPS cell
Nanopillar plate
Drug screening

ABSTRACT

Although it is expected that hepatocyte-like cells differentiated from human embryonic stem (ES) cells or induced pluripotent stem (iPS) cells will be utilized in drug toxicity testing, the actual applicability of hepatocyte-like cells in this context has not been well examined so far. To generate mature hepatocyte-like cells that would be applicable for drug toxicity testing, we established a hepatocyte differentiation method that employs not only stage-specific transient overexpression of hepatocyte-related transcription factors but also a three-dimensional spheroid culture system using a Nanopillar Plate. We succeeded in establishing protocol that could generate more matured hepatocyte-like cells than our previous protocol. In addition, our hepatocyte-like cells could sensitively predict drug-induced hepatotoxicity, including reactive metabolite-mediated toxicity. In conclusion, our hepatocyte-like cells differentiated from human ES cells or iPS cells have potential to be applied in drug toxicity testing.

1. Introduction

Hepatocyte-like cells that are generated from human embryonic stem cells (hESCs) [1] or human induced pluripotent stem cells (hiPSCs) [2] are expected to be used in drug screening instead of primary (or cryopreserved) human hepatocytes (PHs). We recently demonstrated that stage-specific transient transduction of transcription factors, in addition to treatment with optimal growth factors and cytokines, is useful for promoting hepatic differentiation [3–6]. The hepatocyte-like cells, which have many hepatocyte characteristics (the abilities to uptake low-density lipoprotein and Indocyanine green, store glycogen, and synthesize urea) and drug metabolism capacity, were generated from hESCs/hiPSCs by combinational transduction of FOXA2 and HNF1α [6]. However, further maturation of the hepatocyte-like cells is required because their hepatic characteristics, such as drug metabolism capacity, are lower than those of PHs [6].

To promote further maturation of the hepatocyte-like cells, we subjected them to three-dimensional (3D) spheroid cultures. It is known that various 3D culture conditions (such as Algimatrix scaffolds [7], cell sheet technology [8], galactose-carrying substrata [9], and basement membrane substratum [10]) are useful for the maturation of the hepatocyte-like cells. Nanopillar Plate technology [11] used in the present study makes it easy to control the configuration of the spheroids. The Nanopillar Plate has an arrayed μm-scale hole structure at the bottom of each well, and nanopillars were aligned further at the bottom of the respective holes. The seeded cells evenly drop into the holes, then migrate and aggregate on top surface of the nanopillars, thus likely to form the uniform spheroids in each hole. Not only 3D spheroid cultures [12] but also Matrigel overlay cultures [13] are useful for maintaining the hepatocyte characteristics of PHs. Therefore, we employed both 3D

* Corresponding author. Laboratory of Biochemistry and Molecular Biology, Graduate School of Pharmaceutical Sciences, Osaka University, 1-6 Yamadaoka, Suita, Osaka 565-0871, Japan. Tel.: +81 6 6879 8185; fax: +81 6 6879 8186.
E-mail address: mizuguch@phs.osaka-u.ac.jp (H. Mizuguchi).

0142-9612/$ – see front matter © 2012 Elsevier Ltd. All rights reserved.
http://dx.doi.org/10.1016/j.biomaterials.2012.11.029

spheroid culture and Matrigel overlay culture systems to promote hepatocyte maturation of the hepatocyte-like cells.

The hepatocyte-like cells generated from hESCs/hiPSCs are expected to be used in drug development. To the best of our knowledge, however, few studies have tried to predict widespread drug-induced cytotoxicity *in vitro* using the hepatocyte-like cells. To precisely determine the applicability of the hepatocyte-like cells to drug screening, it is necessary to investigate the responses of these hepatocyte-like cells to many kinds of hepatotoxic drugs.

In this study, 3D spheroid and Matrigel overlay cultures of the hepatocyte-like cells were performed to promote hepatocyte maturation. The gene expression analysis of cytochrome P450 (CYP) enzymes, conjugating enzymes, hepatic transporters, and hepatic nuclear receptors in the 3D spheroid-cultured hESC- or hiPSC-derived hepatocyte-like cells (3D ES-hepa or 3D iPS-hepa), were analyzed. In addition, CYP induction potency and drug metabolism capacity were estimated in the 3D ES/iPS-hepa. To determine the suitability of these cells for drug screening, we examined whether the drug-induced cytotoxicity is induced by treatment of various kinds of hepatotoxic drugs in 3D ES/iPS-hepa.

2. Materials and methods

2.1. hESCs and hiPSCs culture

A hESC line, H1 and H9 (WiCell Research Institute), was maintained on a feeder layer of mitomycin C-treated mouse embryonic fibroblasts (Millipore) with Repro Stem medium (Repro CELL) supplemented with 5 ng/ml fibroblast growth factor 2 (FGF2) (Sigma). Both H1 and H9 were used following the Guidelines for Derivation and Utilization of Human Embryonic Stem Cells of the Ministry of Education, Culture, Sports, Science and Technology of Japan and furthermore, and the study was approved by Independent Ethics Committee.

Three human iPSC lines were provided from the JCRB Cell Bank (Tic, JCRB Number: JCRB1331; Dotcom, JCRB Number: JCRB1327; Toe, JCRB Number: JCRB1338) [14,15]. These human iPSC lines were maintained on a feeder layer of mitomycin C-treated mouse embryonic fibroblasts with iPSellon (Cardio) supplemented with 10 ng/ml FGF2. Other three human iPSC lines, 201B6, 201B7 and 253G1 were kindly provided by Dr. S. Yamanaka (Kyoto University) [2]. These human iPSC lines were maintained on a feeder layer of mitomycin C-treated mouse embryonic fibroblasts with Repro Stem supplemented with 5 ng/ml FGF2.

2.2. In vitro differentiation

Before the initiation of cellular differentiation, the medium of hESCs was exchanged into a defined serum-free medium, hESF9, and cultured as previously reported [16]. The differentiation protocol for the induction of definitive endoderm cells, hepatoblasts, and hepatocytes was based on our previous reports with some modifications [3–5,17]. Briefly, in mesendoderm differentiation, hESCs were dissociated into single cells by using Accutase (Millipore) and cultured for 2 days on Matrigel (BD Biosciences) in differentiation hESF-DIF medium which contains 100 ng/ml Activin A (R&D Systems) and 10 ng/ml bFGF (hESF-DIF medium was purchased from Cell Science & Technology Institute; differentiation hESF-DIF medium was supplemented with 10 μg/ml human recombinant insulin, 5 μg/ml human apotransferrin, 10 μM 2-mercaptoethanol, 10 μM ethanolamine, 10 μM sodium selenite, and 0.5 mg/ml bovine fatty acid free serum albumin [all from sigma]). To generate definitive endoderm cells, the mesendoderm cells were transduced with 3000 vector particle (VP)/cell of Ad-FOXA2 for 1.5 h on day 2 and cultured until day 6 on Matrigel in differentiation hESF-DIF medium supplemented with 100 ng/ml Activin A and 10 ng/ml bFGF. For induction of hepatoblasts, the DE cells were transduced with each 1500 VP/cell of Ad-FOXA2 and Ad-HNF1α for 1.5 h on day 6 and cultured for 3 days on Matrigel in hepatocyte culture medium (HCM) (Lonza) supplemented with 30 ng/ml bone morphogenetic protein 4 (BMP4) (R&D Systems) and 20 ng/ml FGF4 (R&D Systems). In hepatic expansion, the hepatoblasts were transduced with each 1500 VP/cell of Ad-FOXA2 and Ad-HNF1α for 1.5 h on day 9 and cultured for 3 days on Matrigel in HCM supplemented with 10 ng/ml hepatocyte growth factor (HGF), 10 ng/ml FGF1, 10 ng/ml FGF4, and 10 ng/ml FGF10 (all from R&D Systems). To perform hepatocyte maturation on Nanopillar Plate (a prototype multi-well culturing plate for spheroid culture developed and prepared by Hitachi High-Technologies Corporation) shown in Fig. 1B, the cells were seeded at 2.5×10^5 cells/cm^2 (Fig. S1) in hepatocyte culture medium (Fig. S2) supplemented with 10 ng/ml HGF, 10 ng/ml FGF1, 10 ng/ml FGF4, and 10 ng/ml FGF10 on day 11. In the first stage of hepatocyte maturation (from day 12 to day 25), the cells were cultured for 13 days on Matrigel in HCM supplemented with 20 ng/ml HGF, 20 ng/ml oncostatin M (OsM), 10 ng/ml FGF4, and 10^{-6} M dexamethasone (DEX). In the second stage of hepatocyte maturation (from day 25 to day 35), Matrigel was overlaid on the hepatocyte-like cells. Matrigel were diluted to a final concentration of 0.25 mg/ml with William's E medium (Invitrogen) containing 4 mM L-glutamine, 50 ug/ml gentamycin sulfate, 1 × ITS (BD Biosciences), 20 ng/ml OsM, and 10^{-6} M DEX. The culture medium was aspirated, and then the Matrigel solution (described above) was overlaid on the hepatocyte-like cells. The cells were incubated overnight, and the medium was replaced with HCM supplemented with 20 ng/ml OsM and 10^{-6} M DEX.

2.3. Adenovirus (Ad) vectors

Ad vectors were constructed by an improved *in vitro* ligation method [18,19]. The human EF-1α promoter-driven LacZ-, FOXA2-, or HNF1α-expressing Ad vectors (Ad-LacZ, Ad-FOXA2, or Ad-HNF1α, respectively) were constructed previously [3,4,20]. All of Ad vectors contain a stretch of lysine residue (K7) peptides in the C-terminal region of the fiber knob for more efficient transduction of hESCs, hiPSCs, and DE cells, in which transfection efficiency was almost 100%, and purified as described previously [3–5]. The vector particle (VP) titer was determined by using a spectrophotometric method [21].

2.4. Flow cytometry

Single-cell suspensions of hESC/hiPSC-derived cells were fixed with 2% paraformaldehyde (PFA) at 4°C for 20 min, and then incubated with the primary antibody (described in Table S1), followed by the secondary antibody (described in Table S1). Flow cytometry analysis was performed using a FACS LSR Fortessa flow cytometer (BD Biosciences).

2.5. RNA isolation and reverse transcription-polymerase chain reaction (RT-PCR)

Total RNA was isolated from hESCs or hiPSCs and their derivatives using ISOGENE (Nippon Gene). cDNA was synthesized using 500 ng of total RNA with a Superscript VILO cDNA synthesis kit (Invitrogen). Real-time RT-PCR was performed with Taqman gene expression assays (Applied Biosystems) or SYBR Premix Ex Taq (TaKaRa) using an ABI PRISM 7000 Sequence Detector (Applied Biosystems). Relative quantification was performed against a standard curve and the values were normalized against the input determined for the housekeeping gene, glyceraldehyde 3-phosphate dehydrogenase (GAPDH). The primer sequences used in this study are described in Table S2.

2.6. Immunohistochemistry

The cells were fixed with 4% PFA. After incubation with 1% Triton X-100, blocking with Blocking One (Nakalai tesque), the cells were incubated with primary antibody (describe in Table S1) at 4°C for over night, followed by incubation with a secondary antibody (described in Table S1) at room temperature for 1 h.

2.7. ELISA

The hESCs or hiPSCs were differentiated into hepatocytes as described in Fig. 1A. The culture supernatants, which were incubated for 24 h after fresh medium was added, were collected and analyzed for the amount of ALB secretion by ELISA. ELISA kits for ALB were purchased from Bethyl. ELISA was performed according to the manufacturer's instructions. The amount of ALB secretion was calculated according to each standard followed by normalization to the protein content per well.

2.8. Urea secretion

The hESCs or hiPSCs were differentiated into hepatocytes as described in Fig. 1A. The culture supernatants, which were incubated for 24 h after fresh medium was added, were collected and analyzed for the amount of urea secretion. Urea measurement kits were purchased from BioAssay Systems. The experiment was performed according to the manufacturer's instructions. The amount of urea secretion was calculated according to each standard followed by normalization to the protein content per well.

2.9. Canalicular secretory assay

At cellular differentiation, the hepatocyte-like cell spheroids were treated with 5 mM choly-lysyl-fluorescein (CLF) (BD Biosciences) for 30 min. The cells were washed with culture medium, and then observed by fluorescence microscope. To inhibit the function of BSEP, the cells were pretreated with Cyclosporin A 24 h before of the CLF treatment.

2.10. Assay for CYP activity and CYP induction

To measure the cytochrome P450 2C9 and 3A4 activity of the cells, we performed lytic assays by using a P450-GloTM CYP2C9 (catalog number; V8791) and

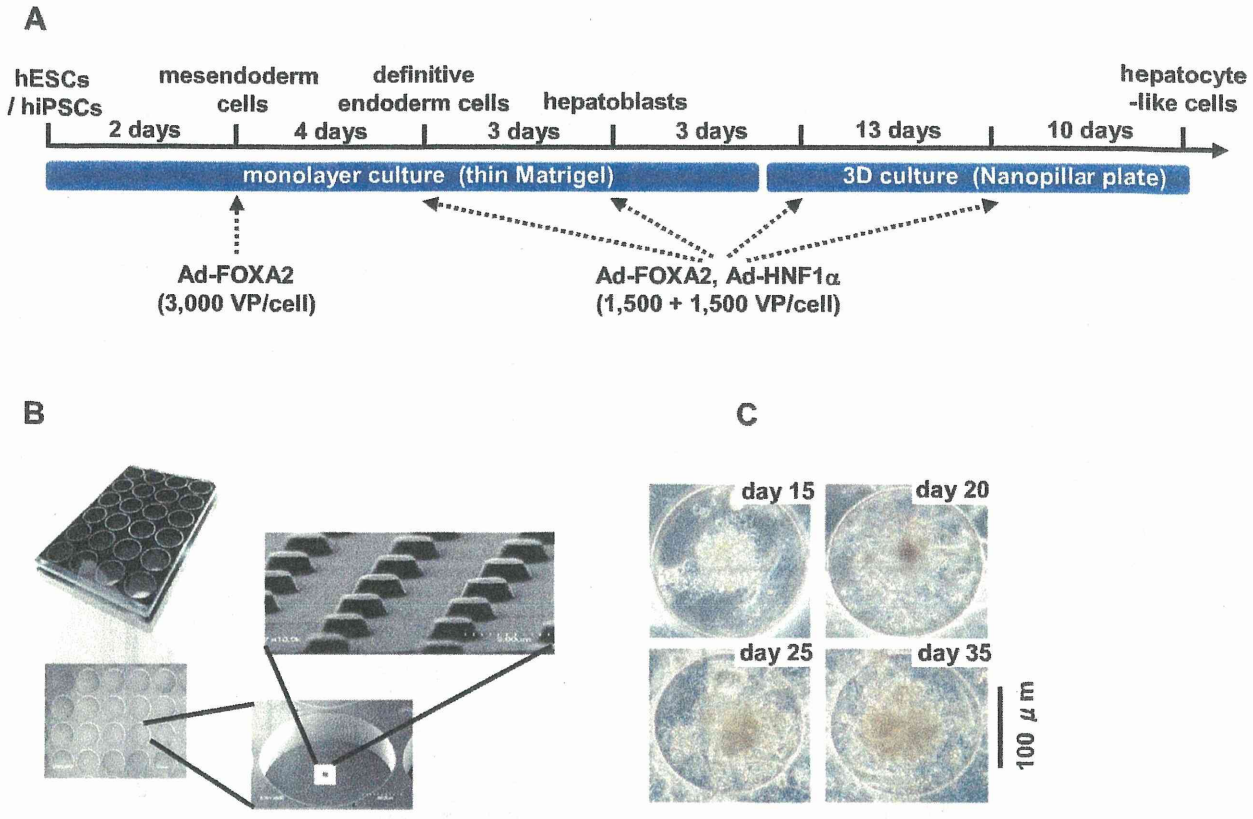

Fig. 1. Hepatocyte-like cells were differentiated from hESCs/hiPSCs by using Nanopillar Plate. (A) The procedure for differentiation of hESCs into 3D ES/iPS-hepa via mesendoderm cells, definitive endoderm cells, and hepatoblasts is presented schematically. In the differentiation, not only the addition of growth factors but also stage-specific transient transduction of both FOXA2- and HNF1α-expressing Ad vector (Ad-FOXA2 and Ad-HNF1α, respectively) was performed. The cellular differentiation procedure is described in detail in the materials and methods section. (B) Photograph display of a 24-well format Nanopillar Plate and its microstructural appearances of the hole and pillar structure. (C) Phase-contrast micrographs of the hESC-hepa spheroids on the Nanopillar Plate are shown. Scale bar represents 100 μm.

3A4 (catalog number; V9001) Assay Kit (Promega), respectively. We measured the fluorescence activity with a luminometer (Lumat LB 9507; Berthold) according to the manufacturer's instructions. The CYP activity was normalized with the protein content per well.

To measure CYP2C9 and 3A4 induction potency, the CYP activity was measured by using a P450-GloTM CYP2C9 and 3A4 Assay Kit, respectively. The cells were treated with rifampicin, which is known to induce both CYP2C9 and 3A4, at a final concentration of 10 μM for 48 h. The cells were also treated with Ketoconazole (Sigma) or Sulfaphenazole (Sigma), which are inhibitors for CYP3A4 or 2C9, at a final concentration of 1 μM or 2 μM, respectively, for 48 h. Controls were treated with DMSO (final concentration 0.1%). Inducer compounds were replaced daily.

2.11. Cell viability tests

Cell viability was assessed by the WST-8 assay kit (Dojindo) in Fig. 2D. After treatment with test compounds, such as Acetaminophen (Wako), Allopurinol (Wako), Amiodaron (Sigma), Benzbromarone (Sigma), Clozapine (Wako), Cyclizine (MP bio), Dantrolene (Wako), Desipramine (Wako), Disufliram (Wako), Erythromycin (Wako), Felbamate (Sigma), Flutamide (Wako), Isoniazid (Sigma), Labetalol (Sigma), Lefunomide (Sigma), Maprotiline (Sigma), Nefazodone (Sigma), Nitrofurantoin (Sigma), Sulindac (Wako), Tacrine (Sigma), Tebinafine (Wako), Tolcapone (TRC), Troglitazone (Wako), and Zafirlukast (Cayman) for 24 h, the cell viability was measured. The cell viability of the 3D iPSC-hepa were assessed by WST-8 assay after 24 h exposure to different concentrations of Aflatoxin B1 (Sigma) and Benzbromarone in the presence or absence of the CYP3A4 or 2C9 inhibitor, Ketoconazole (1 μM) or Sulfaphenazole (10 μM), respectively. The control refers to incubations in the absence of test compounds and was considered as 100% viability value. Controls were treated with DMSO (final concentration 0.1%). ATP assay (BioAssay Systems), Alamar Blue assay (Invitrogen), and Crystal Violet (Wako) staining assay were performed according to the manufacturer's instructions.

2.12. Primary human hepatocytes

Three lots of cryopreserved human hepatocytes (lot Hu8072 [CellzDirect], HC2-14, and HC10-101 [Xenotech]) were used. These three lots of crypreserved human hepatocytes were cultured according to our previous report [5].

2.13. Statistical analysis

Statistical analysis was performed using the unpaired two-tailed Student's *t*-test. All data are represented as means ± SD (n = 3).

3. Results

The 3D ES/iPS-hepa were generated from hESCs/hiPSCs as shown in Fig. 1A. Hepatocyte differentiation of hESCs/hiPSCs was efficiently promoted by stage-specific transient transduction of FOXA2 and HNF1α in addition to the treatment with appropriate soluble factors (growth factors and cytokines) [6]. On day 11, the hESC-derived cells were seeded at 2.5×10^5 cells/cm^2 (Fig. S1) on Nanopillar Plate (Fig. 1B), in hepatocyte culture medium (Fig. S2) to promote hepatocyte maturation. In addition, Matrigel was overlaid on the 3D ES-hepa to promote further hepatocyte maturation. The 3D ES-hepa with compact morphology that were adhesive to the substratum and had an optimal size (approximately 100 μm in diameter) were formed by using the Nanopillar Plate (Fig. 1C). The spheroids seem to be stable because they could be cultured for more than 20 days. We have confirmed that more than 90% of the cells that constitute the spheroids were alive, indicating that the necrotic centers are absent.

To investigate whether or not a 3D spheroid culture could promote hepatocyte maturation of the hepatocyte-like cells, various hepatocyte characteristics of the 3D ES/iPS-hepa were compared with those of the monolayer-cultured hESC- or hiPSC-derived hepatocyte-like cells (mono ES-hepa or mono iPS-hepa). The gene expression level of *ALB* peaked on day 20 in the mono ES-hepa, and then it was dramatically decreased after day 25 (Fig. 2A). In contrast, the gene expression level of *ALB* was

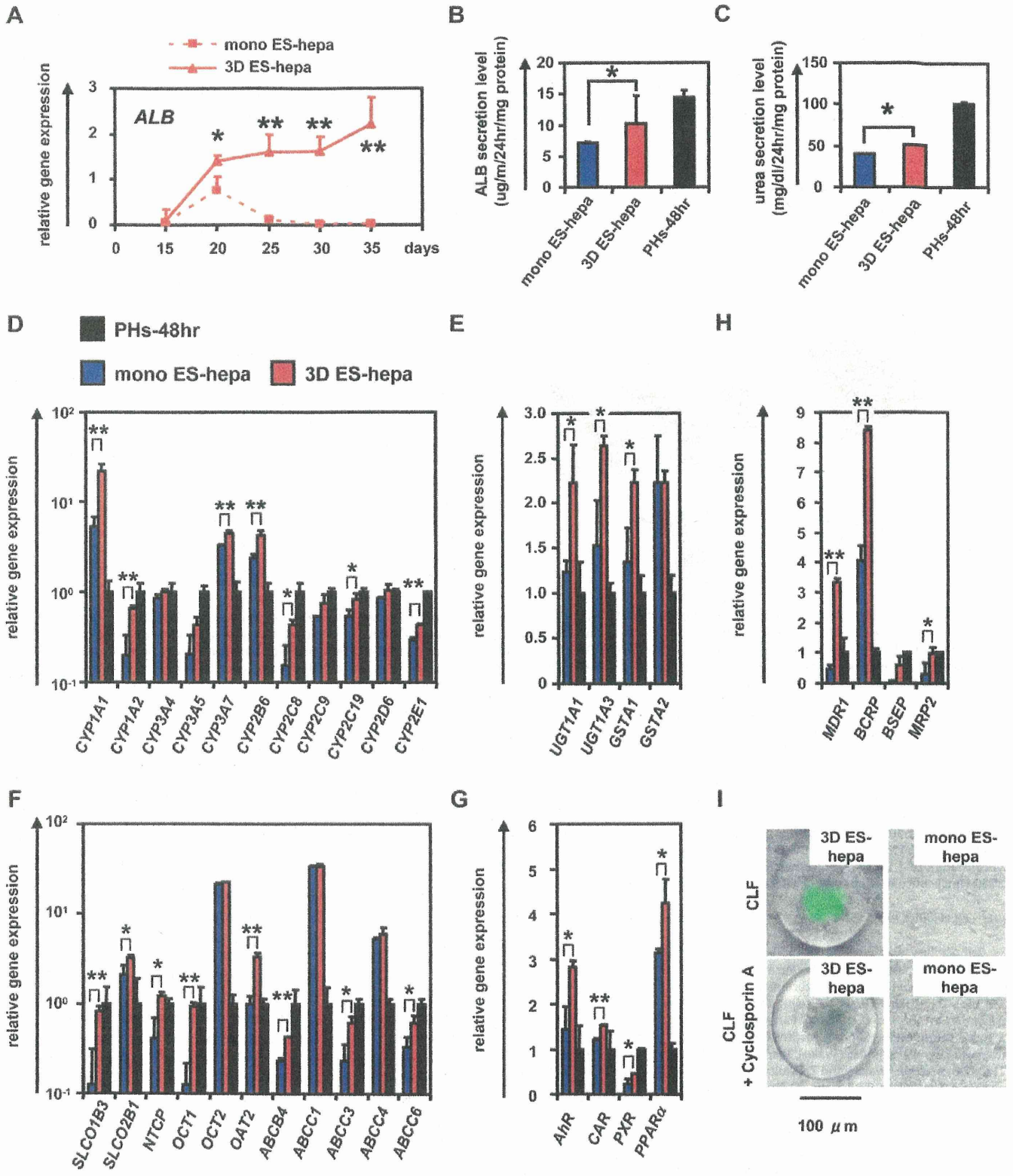

Fig. 2. Hepatocyte functions in hESC-derived hepatocyte-like cells were enhanced by using Nanopillar Plate. (A) The gene expression levels of *ALB* were measured by real-time RT-PCR on day 15, 20, 25, 30, and 35. On the *y* axis, the gene expression levels in PHs (three lots of PHs were used in all studies), which were cultured for 48 h after plating (PHs-48hr), were taken as 1.0. (B, C) The amount of ALB (B) and urea (C) secretion were examined in the mono ES-hepa (day 20), the 3D ES-hepa (day 35), and PHs-48hr. (D–H) The gene expression levels of CYP enzymes (D), conjugating enzymes (E), hepatic transporters (F), hepatic nuclear receptors (G), and bile canaliculi transporters (H) were examined by real-time RT-PCR in the mono ES-hepa, the 3D ES-hepa, and PHs-48hr. On the *y* axis, the expression levels in PHs-48hr were taken as 1.0. (I) The ability of bile acid uptake and efflux was examined in the mono ES-hepa and 3D ES-hepa. Choly-lysyl-fluorescein (CLF) (5 μM) was used for the observation of bile canaliculi uptake and efflux. To inhibit transportation by BSEP, the cells were pretreated with 1 μM Cyclosporin A. $^{*}P < 0.05$; $^{**}P < 0.01$.

moderately increased in the 3D ES-hepa until day 35 (Fig. 2A). These results suggest that the hepatocyte functions of the 3D ES-hepa are sustained for more than 2 weeks on the Nanopillar Plate, although those of the mono ES-hepa are rapidly devitalized (Fig. 2A and Fig. S4). Other hepatocyte characteristics, such as ability of ALB and urea secretion and gene expression levels of hepatocyte-related markers in the 3D ES-hepa were compared with those of the mono ES-hepa (Fig. 2B–H). Because the gene expression level of *ALB* in the 3D ES-hepa was the highest on day 35 and that in mono ES-hepa was the highest on day 20, various hepatocyte characteristics were compared on day 35 or day 20, respectively. The amount of ALB (Fig. 2B) and urea (Fig. 2C) secretion in the 3D ES-hepa was higher than those of the mono ES-hepa. The gene expression levels of CYP enzymes (Fig. 2D), conjugating enzymes (Fig. 2E), hepatic transporters (Fig. 2F), hepatic nuclear receptors (Fig. 2G), and hepatic transcription factors (Fig. S5) in the 3D ES-hepa were higher than those in the mono ES-hepa. The expression levels of most of the genes in the 3D ES-hepa were higher than those in the mono ES-hepa. Because the previous study [11] showed that hepatocyte spheroids expressed hepatocyte transporters similar to those of the bile canaliculi in native liver tissue, the gene expression levels of bile canaliculi transporters (Fig. 2H), as well as the ability of bile acid uptake and efflux, (Fig. 2I) were examined in the 3D ES-hepa. The gene expression levels of bile canaliculi transporters were increased in the 3D ES-hepa compared with those of mono ES-hepa and PHs (Fig. 2H). The bile canaliculi formation was visualized by BSEP fluorescent substrate: Cholyl-lysyl-fluorescein (CLF), which is inhibited by BSEP

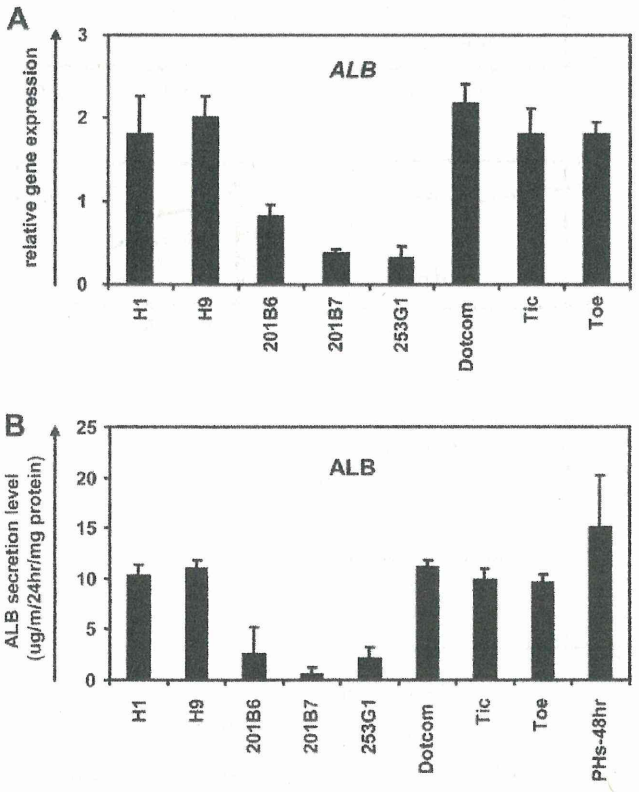

Fig. 3. Comparison of the hepatic differentiation capacities of various hESC and hiPSC lines hESCs (H1 and H9) and hiPSCs (201B6, 201B7, 253G1, Dotcom, Tic, and Toe) were differentiated into the 3D ES/iPS-hepa as described in Fig. 1A. (A) On day 20, the gene expression level of *ALB* was examined by real-time RT-PCR. On the *y* axis, the gene expression level of *ALB* in PHs-48hr was taken as 1.0. (B) On day 20, the amount of ALB secretion was examined by ELISA. The amount of ALB secretion was calculated according to each standard followed by normalization to the protein content per well.

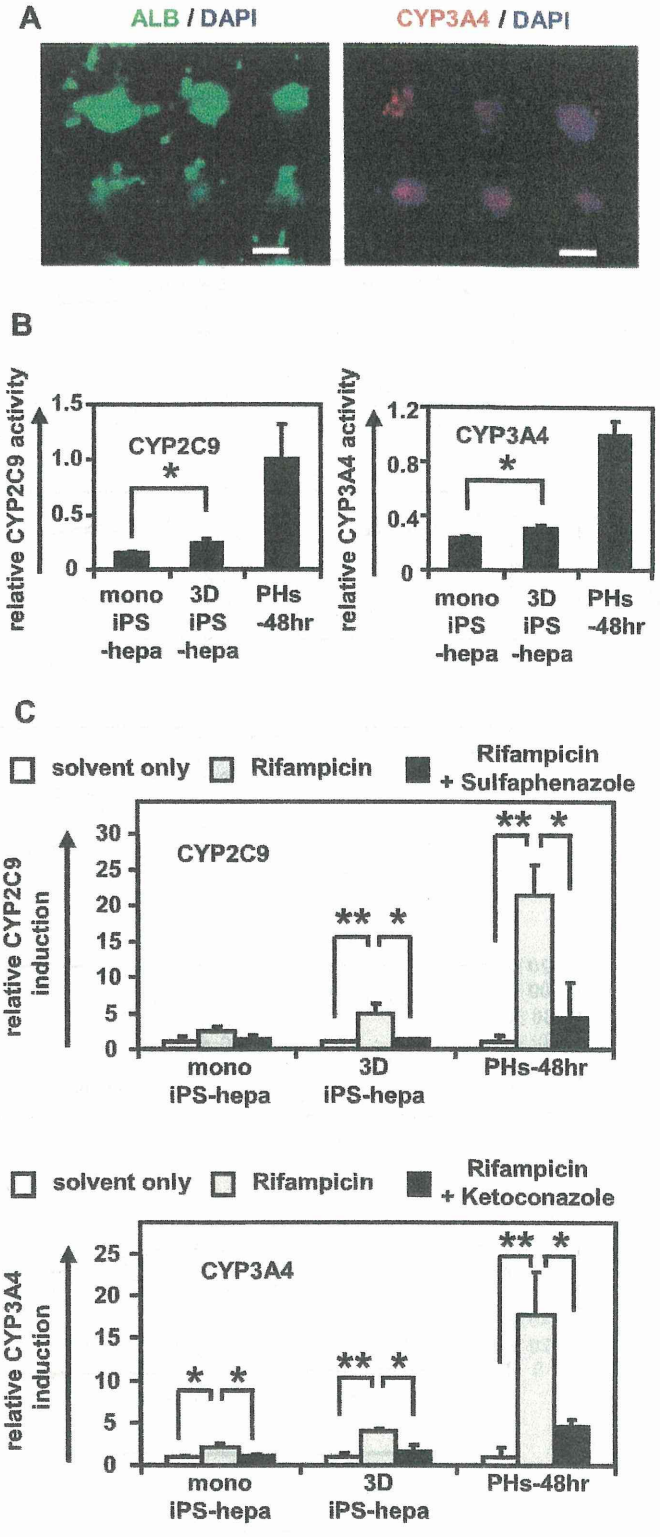

Fig. 4. Drug metabolism capacity and CYP induction potency were examined in the 3D iPS-hepa. (A) The 3D iPS-hepa (day 35) were subjected to immunostaining with anti-ALB (green) or CYP3A4 (red) antibodies. Nuclei were counterstained with DAPI (blue). Scale bar represents 100 μm. (B) The CYP activity was measured in the mono iPS-hepa (day 20), the 3D iPS-hepa (day 35), and PHs-48hr. On the *y* axis, the CYP activity in PHs-48hr was taken as 1.0. (C) Induction of CYP2C9 (left) or CYP3A4 (right) by DMSO (solvent only; white bar), Rifampicin (gray bar), or rifampicin and CYP inhibitor (Sulfaphenazole or Ketoconazole, black bar) in the mono iPS-hepa, the 3D iPS-hepa, and PHs-48hr. On the *y* axis, the CYP activity of the cells that have been cultured in DMSO-containing medium was taken as 1.0. $^{*}P < 0.05$; $^{**}P < 0.01$.

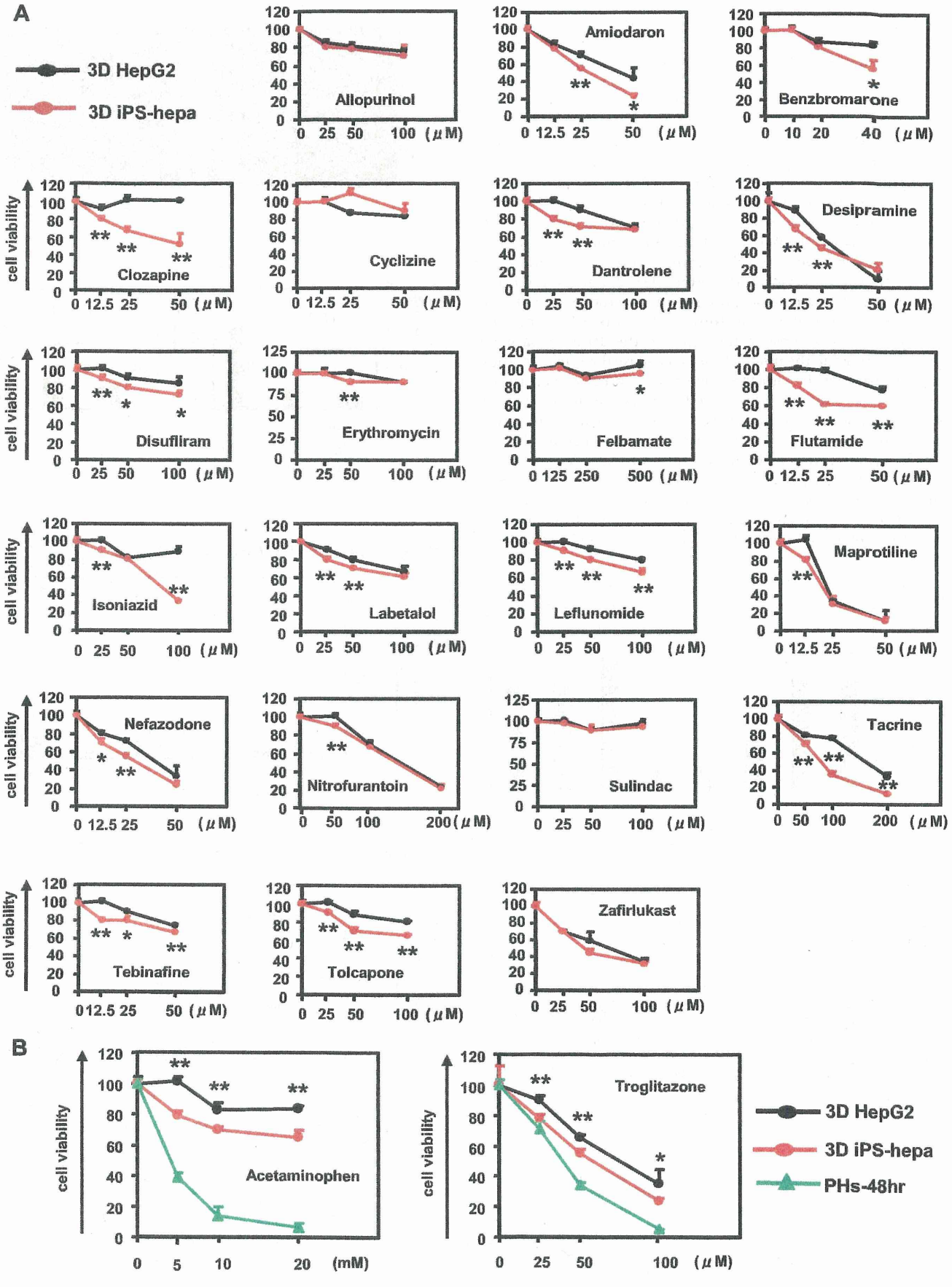
A
3D HepG2
3D iPS-hepa
Allopurinol
Amiodaron
Benzbromarone
Clozapine
Cyclizine
Dantrolene
Desipramine
Disufliram
Erythromycin
Felbamate
Flutamide
Isoniazid
Labetalol
Leflunomide
Maprotiline
Nefazodone
Nitrofurantoin
Sulindac
Tacrine
Tebinafine
Tolcapone
Zafirlukast
B
Acetaminophen
Troglitazone
3D HepG2
3D iPS-hepa
PHs-48hr
cell viability
(μM)
(mM)

inhibitor Cyclosporin A [22,23]. More CLF was accumulated in the 3D ES-hepa than in the mono ES-hepa (Fig. 2I *upper panel*). Moreover, CLF accumulation was inhibited by Cyclosporin A treatment only in the 3D ES-hepa (Fig. 2I *lower panel*), demonstrating that the functionality of BSEP transporter in 3D ES-hepa was greater than that in mono ES-hepa. These results suggested that hepatocyte maturation was promoted by the culture on the Nanopillar Plate. It is likely that, compared to the monolayer culture condition, the 3D spheroid-culture condition is more similar to the *in vivo* condition.

It is important to select an hESC/hiPSC line that has a strong ability to differentiate into hepatocyte-like cells in the case of medical applications such as drug screening. In this study, two hESC lines and six hiPSC lines were differentiated into the hepatocyte-like cells, and then their gene expression levels of *ALB* (Fig. 3A) and ALB secretion levels (Fig. 3B) were compared. These results suggest that the iPSC line, Dotcom, was the suitable cell line for hepatocyte maturation. Therefore, the iPSC line, Dotcom, was used to examine the possibility of the 3D iPS-hepa for drug screening. The drug metabolism capacity and the CYP induction potency of the 3D iPS-hepa were compared with those of the mono iPS-hepa. We confirmed the expression of ALB and CYP3A4 protein in the 3D ES-hepa (Fig. 4A). The activity levels of CYP enzymes in the 3D iPS-hepa were measured according to the metabolism of the CYP2C9 or CYP3A4 substrates (Fig. 4B); the levels were higher than those of the mono iPS-hepa (Fig. 4B). We further tested the induction of CYP2C9 and CYP3A4 by chemical stimulation (rifampicin was used as a CYP2C9 or CYP3A4 inducer). Compared with mono iPS-hepa, the 3D iPS-hepa produced more metabolites in response to chemical stimulation (Fig. 4C). In addition, the CYP induction was inhibited by using CYP2C9 or CYP3A4 inhibitor (Sulfaphenazole or Ketoconazole, respectively). These results indicated that drug metabolism capacity and CYP induction potency in 3D iPS-hepa were higher than those in mono iPS-hepa.

Many researchers have tried to predict the drug-induced cytotoxicity *in vitro* using hepatocarcinoma-derived cells such as HepG2 cells [24,25]. HepG2 cells are less expensive than PHs and the reproducible experiments are easier to perform than they are with PHs, although 30% of the compounds were incorrectly classified as nontoxic [24,25]. To overcome these problems, hESC/hiPSC-derived hepatocyte-like cells are expected to be used to predict drug-induced cytotoxicity. To examine its applicability to drug screening, the 3D iPS-hepa were treated with various drugs, that cause hepatotoxicity. WST-8 assay was performed to evaluate cell viability (Fig. S6). The susceptibility of the 3D iPS-hepa to most of the hepatotoxic drugs was higher than that of the mono iPS-hepa (Fig. S7). Compared to the mono iPS-hepa, the 3D iPS-hepa were more suitable tools for drug screening. Next, the susceptibility of the 3D iPS-hepa to the hepatotoxic drugs was compared with that of the 3D spheroid cultured HepG2 cells (3D HepG2; the hepatocyte functions of 3D HepG2 cells are higher than those of monolayer cultured HepG2 cells [Fig. S8]). With most of the drugs, the cell viability of the 3D iPS-hepa was lower than that of the 3D HepG2 (Fig. 5A). These results indicated that the 3D iPS-hepa are more valuable tools for drug screening than the 3D HepG2. However, the susceptibility of the 3D iPS-hepa to Acetaminophen and Troglitazone was lower than that of the PHs which were cultured for 48 h after the cells were plated (Fig. 5B). These results might be due to the lower activity levels of CYPs in 3D iPS-hepa as compared as those in PHs. Taken together, 3D iPS-hepa are more valuable tools for drug screening than the 3D HepG2, although further maturation of 3D iPS-hepa is still required for 3D iPS-hepa to be an alternative cell source of PHs in the drug screening.

To examine whether drug-induced cytotoxicity is caused by CYP metabolites in 3D iPS-hepa, Aflatoxin B1 (mainly metabolized by CYP3A4 [26]) and Benzbromarone (mainly metabolized by CYP2C9 [27]) were treated in the presence or absence of a CYP3A4 and a 2C9 inhibitor, Ketoconazole and Sulfaphenazole, respectively (Fig. 6). The cell viability of 3D iPS-hepa was partially rescued by treatment with the CYP inhibitor. These results indicated that drug-induced cytotoxicity was caused by CYP metabolites of Aflatoxin B1 and Benzbromarone.

4. Discussion

Recently, it has been expected that human pluripotent stem cells and their derivatives, including hepatocyte-like cells, will be utilized in applications for the safety assessment of drugs. We have previously reported that combinational overexpression of SOX17, HEX, and HNF4α, or combinational overexpression of FOXA2 and HNF1α could promote hepatocyte differentiation [5,6]. However, the drug metabolism capacity of the hepatocyte-like cells generated by our previous protocol was still lower than that of primary human hepatocytes [6]. To generate more matured hepatocyte-like cells as compared with our previous protocol, we established a hepatocyte differentiation method employing not only stage-specific transient overexpression of hepatocyte-related transcription factors but also a 3D culture systems using a Nanopillar Plate, was established. Although the use of hepatocyte-like cells generated from hESCs/hiPSCs in application for drug toxicity testing has begun to be focused, to the best of our knowledge, there have been few studies that have investigated whether hepatocyte-like cells could predict many kinds of drug-induced toxicity.

3D culture spheroids were generated from hESCs/hiPSCs by using a Nanopillar Plate. The diameter of the spheroids was approximately 100 μm on day 35 of differentiation (Fig. 1C). Because it is known that the no-oxygen limitation would take place in spheroids up to 100 μm in diameter [28], the size of the spheroid might be important to generate spheroids with high viability. A Nanopillar Plate has a potential to regulate the spheroid diameter simply by culturing under optimized seeding condition, on its suitably designed pillar and hole structure [11]. Therefore, a Nanopillar Plate would be a suitable environment for the generation of 3D ES/iPS-hepa that show high viability and possess high level of hepatocellular functions.

The levels of many hepatocyte functions, such as ALB secretion ability (Fig. 2B), urea secretion ability (Fig. 2C), hepatocyte-related gene expressions (Fig. 2D–H), drug metabolism capacity (Fig. 4B), and CYP induction potency (Fig. 4C), of 3D ES/iPS-hepa were higher than those of mono ES/iPS-hepa. This might have been because the structural and functional polarity, which can be seen in the naïve environment of hepatocytes, of the hepatocyte-like cells was configured by a 3D culturing condition. Previous studies have shown that a 3D culture condition is suitable to maintain the hepatic characteristics of the isolated hepatocytes because this condition mimic *in vivo* environment [29,30]. These facts indicated that the 3D culture condition is a more suitable condition for the hepatocyte-like cells than the monolayer culture condition.

Two hES cell lines and six hiPS cell lines were differentiated into the hepatocyte-like cells in this study. The hiPS cell line, Dotcom, seemed to be a suitable cell line for hepatic differentiation (Fig. 3). Because the hepatic differentiation propensity differs among the

Fig. 5. The possibility of applying 3D iPS-hepa to drug testing was examined. (A) The cell viability of the 3D HepG2 (black) and 3D iPSC-hepa (red) were assessed by WST-8 assay after 24 h exposure to different concentrations of 22 test compounds. (B) The cell viability of the 3D HepG2 (black), 3D iPSC-hepa (red), and PHs-48hr (green) were assessed by WST-8 assay after 24 h exposure to different concentrations of Acetaminophen and Troglitazone. Cell viability is expressed as a percentage of cells treated with solvent only. $^{*}P < 0.05$; $^{**}P < 0.01$.

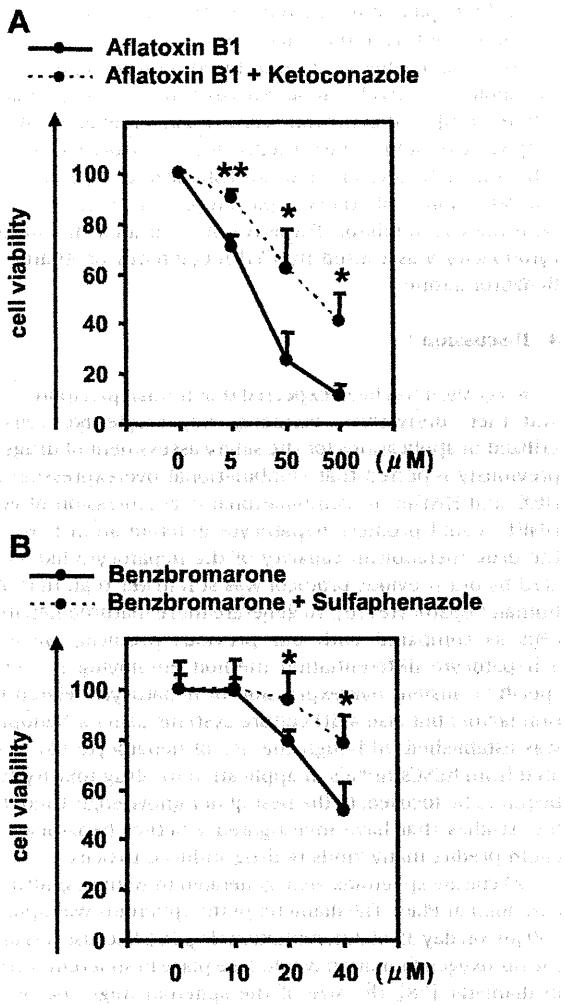

Fig. 6. Drug-induced cytotoxicity in the 3D iPS-hepa is mediated by cytochrome P450. (A, B) The cell viability of the 3D iPSC-hepa was assessed by WST-8 assay after 24 h exposure to different concentrations of (A) Aflatoxin B1 and (B) Benzbromarone in the presence or absence of the CYP3A4 or 2C9 inhibitor, Ketoconazole or Sulfaphenazole, respectively. Cell viability was expressed as the percentage of cells treated with solvent only. $^{*}P < 0.05$; $^{**}P < 0.01$.

hES/hiPS cell lines, it would be important to select an appropriate cell line for medical applications such as drug screening. However, the dominant reason for this hepatic differentiation propensity is not been well known. It would be interesting study to elucidate the mechanism of this propensity.

Although the drug metabolism capacity and CYP induction potency of 3D iPS-hepa were higher than those of mono iPS-hepa (Fig. 4B and C), they were still lower than those of primary human hepatocytes. The hepatic nuclear factors are known to be key molecules in the CYP induction of hepatocytes [30]. Therefore, overexpression of hepatic nuclear factors, which are not abundantly expressed in the hepatocyte-like cells (such as *PXR*), might upregulate the CYP induction potency of the hepatocyte-like cells.

3D iPS-hepa were more sensitive for detection of the drug-induced cytotoxicity than HepG2 cells that are widely used to predict hepatotoxicity [31,32] (Fig. 5). In addition, the decrease of cell viability, which was caused by hepatotoxic drugs, of 3D iPS-hepa was partially rescued by treatment with a CYP inhibitor (Fig. 6). These data suggest that the hepatocyte-like cells could detect the toxicity of the reactive metabolites that were generated by drug metabolizing enzymes such as CYP enzymes. Because in many cases, drug-induced hepatotoxicity is caused by the reactive metabolites produced by drug metabolizing enzymes [33], our finding that the hepatocyte-like cells could detect the toxicity of reactive metabolites should be of great potential for toxicological screening. Moreover, it might be possible to predict idiosyncratic liver toxicity by using hepatocyte-like cells generated from hiPSCs that were established from a patient with a rare CYP polymorphism. However, some compounds did not show any cytotoxicity (such as Cyclizine, Felbamate, and Sulindac) (Fig. 5). To apply the hepatocyte-like cells for wide-spread drug screening, generation of the hepatocyte-like cells are required to detect hepatotoxity in more sensitive manner. Previous studies showed that the depletion of conjugating enzymes [32] or knockdown of Nrf2 [34] expression are useful to upregulate the sensitivity to hepatotoxic drugs. Therefore, these approaches would be useful to generate more sensitive hepatocytes to toxic drugs.

5. Conclusions

In this study, we established the efficient hepatocyte differentiation method which employs not only stage-specific transient overexpression of hepatocyte-related transcription factors but also 3D spheroid culture systems by using Nanopillar Plate. To the best of our knowledge, this is the first study in which the hepatocyte-like cells, having enough hepatocyte functions, mediate drug-induced cytotoxicity against many compounds. Our hepatocyte-like cells differentiated from hESCs or hiPSCs have potential to be applied in drug toxicity testing.

Acknowledgments

We thank Misae Nishijima and Hiroko Matsumura for their excellent technical support. HM, KK, MKF, and TH were supported by grants from the Ministry of Health, Labor, and Welfare of Japan. HM was also supported by Japan Research foundation For Clinical Pharmacology, and The Uehara Memorial Foundation. MKF was also supported by Japan Society for the Promotion of Science Grant-in-Aid for Scientific Research. FS was supported by Program for Promotion of Fundamental Studies in Health Sciences of the National Institute of Biomedical Innovation (NIBIO). We thank Hiromu Yamada (NIBIO) for helpful discussion.

Appendix A. Supplementary data

Supplementary data related to this article can be found at http://dx.doi.org/10.1016/j.biomaterials.2012.11.029.

References

[1] Thomson JA, Itskovitz-Eldor J, Shapiro SS, Waknitz MA, Swiergiel JJ, Marshall VS, et al. Embryonic stem cell lines derived from human blastocysts. Science 1998;282:1145–7.
[2] Takahashi K, Tanabe K, Ohnuki M, Narita M, Ichisaka T, Tomoda K, et al. Induction of pluripotent stem cells from adult human fibroblasts by defined factors. Cell 2007;131:861–72.
[3] Inamura M, Kawabata K, Takayama K, Tashiro K, Sakurai F, Katayama K, et al. Efficient generation of hepatoblasts from human ES cells and iPS cells by transient overexpression of homeobox gene HEX. Mol Ther 2011;19:400–7.
[4] Takayama K, Inamura M, Kawabata K, Tashiro K, Katayama K, Sakurai F, et al. Efficient and directive generation of two distinct endoderm lineages from human ESCs and iPSCs by differentiation stage-specific SOX17 transduction. PLoS One 2011;6:e21780.
[5] Takayama K, Inamura M, Kawabata K, Katayama K, Higuchi M, Tashiro K, et al. Efficient generation of functional hepatocytes from human embryonic stem cells and induced pluripotent stem cells by HNF4alpha transduction. Mol Ther 2012;20:127–37.
[6] Takayama K, Inamura M, Kawabata K, Sugawara M, Kikuchi K, Higuchi M, et al. Generation of metabolically functioning hepatocytes from human pluripotent stem cells by FOXA2 and HNF1alpha transduction. J Hepatol 2012;57:628–36.
[7] Ramasamy TS, Yu JS, Selden C, Hodgson H, Cui W. Application of three-dimensional culture conditions to human embryonic stem cell-derived

definitive endoderm cells enhances hepatocyte differentiation and functionality. Tissue Eng Part A. http://dx.doi.org/10.1089/ten.tea.2012.0190. Available from URL: http://www.ncbi.nlm.nih.gov/pubmed/23003670; 2012.
[8] Nagamoto Y, Tashiro K, Takayama K, Ohashi K, Kawabata K, Sakurai F, et al. The promotion of hepatic maturation of human pluripotent stem cells in 3D co-culture using type I collagen and Swiss 3T3 cell sheets. Biomaterials 2012;33:4526–34.
[9] Meng Q, Haque A, Hexig B, Akaike T. The differentiation and isolation of mouse embryonic stem cells toward hepatocytes using galactose-carrying substrata. Biomaterials 2012;33:1414–27.
[10] Shiraki N, Yamazoe T, Qin Z, Ohgomori K, Mochitate K, Kume K, et al. Efficient differentiation of embryonic stem cells into hepatic cells in vitro using a feeder-free basement membrane substratum. PLoS One 2011;6:e24228.
[11] Takahashi R, Sonoda H, Tabata Y, Hisada A. Formation of hepatocyte spheroids with structural polarity and functional bile canaliculi using nanopillar sheets. Tissue Eng Part A 2010;16:1983–95.
[12] Tong JZ, Sarrazin S, Cassio D, Gauthier F, Alvarez F. Application of spheroid culture to human hepatocytes and maintenance of their differentiation. Biol Cell 1994;81:77–81.
[13] Bi YA, Kazolias D, Duignan DB. Use of cryopreserved human hepatocytes in sandwich culture to measure hepatobiliary transport. Drug Metab Dispos 2006;34:1658–65.
[14] Makino H, Toyoda M, Matsumoto K, Saito H, Nishino K, Fukawatase Y, et al. Mesenchymal to embryonic incomplete transition of human cells by chimeric OCT4/3 (POU5F1) with physiological co-activator EWS. Exp Cell Res 2009;315:2727–40.
[15] Nagata S, Toyoda M, Yamaguchi S, Hirano K, Makino H, Nishino K, et al. Efficient reprogramming of human and mouse primary extra-embryonic cells to pluripotent stem cells. Genes Cells 2009;14:1395–404.
[16] Furue MK, Na J, Jackson JP, Okamoto T, Jones M, Baker D, et al. Heparin promotes the growth of human embryonic stem cells in a defined serum-free medium. Proc Natl Acad Sci U S A 2008;105:13409–14.
[17] Kawabata K, Inamura M, Mizuguchi H. Efficient hepatic differentiation from human iPS cells by gene transfer. Methods Mol Biol 2012;826:115–24.
[18] Mizuguchi H, Kay MA. Efficient construction of a recombinant adenovirus vector by an improved in vitro ligation method. Hum Gene Ther 1998;9:2577–83.
[19] Mizuguchi H, Kay MA. A simple method for constructing E1- and E1/E4-deleted recombinant adenoviral vectors. Hum Gene Ther 1999;10:2013–7.
[20] Tashiro K, Kawabata K, Sakurai H, Kurachi S, Sakurai F, Yamanishi K, et al. Efficient adenovirus vector-mediated PPAR gamma gene transfer into mouse embryoid bodies promotes adipocyte differentiation. J Gene Med 2008;10:498–507.
[21] Maizel Jr JV, White DO, Scharff MD. The polypeptides of adenovirus. I. Evidence for multiple protein components in the virion and a comparison of types 2, 7A, and 12. Virology 1968;36:115–25.
[22] Yasumiba S, Tazuma S, Ochi H, Chayama K, Kajiyama G. Cyclosporin A reduces canalicular membrane fluidity and regulates transporter function in rats. Biochem J 2001;354:591–6.
[23] Roman ID, Fernandez-Moreno MD, Fueyo JA, Roma MG, Coleman R. Cyclosporin A induced internalization of the bile salt export pump in isolated rat hepatocyte couplets. Toxicol Sci 2003;71:276–81.
[24] Rodriguez-Antona C, Donato MT, Boobis A, Edwards RJ, Watts PS, Castell JV, et al. Cytochrome P450 expression in human hepatocytes and hepatoma cell lines: molecular mechanisms that determine lower expression in cultured cells. Xenobiotica 2002;32:505–20.
[25] Hewitt NJ, Hewitt P. Phase I and II enzyme characterization of two sources of HepG2 cell lines. Xenobiotica 2004;34:243–56.
[26] Gallagher EP, Kunze KL, Stapleton PL, Eaton DL. The kinetics of aflatoxin B1 oxidation by human cDNA-expressed and human liver microsomal cytochromes P450 1A2 and 3A4. Toxicol Appl Pharmacol 1996;141:595–606.
[27] Lee MH, Graham GG, Williams KM, Day RO. A benefit-risk assessment of benzbromarone in the treatment of gout. Was its withdrawal from the market in the best interest of patients? Drug Saf 2008;31:643–65.
[28] Glicklis R, Merchuk JC, Cohen S. Modeling mass transfer in hepatocyte spheroids via cell viability, spheroid size, and hepatocellular functions. Biotechnol Bioeng 2004;86:672–80.
[29] Kim K, Ohashi K, Utoh R, Kano K, Okano T. Preserved liver-specific functions of hepatocytes in 3D co-culture with endothelial cell sheets. Biomaterials 2012;33:1406–13.
[30] Khetani SR, Bhatia SN. Microscale culture of human liver cells for drug development. Nat Biotechnol 2008;26:120–6.
[31] Iwamura A, Fukami T, Hosomi H, Nakajima M, Yokoi T. CYP2C9-mediated metabolic activation of losartan detected by a highly sensitive cell-based screening assay. Drug Metab Dispos 2011;39:838–46.
[32] Hosomi H, Akai S, Minami K, Yoshikawa Y, Fukami T, Nakajima M, et al. An in vitro drug-induced hepatotoxicity screening system using CYP3A4-expressing and gamma-glutamylcysteine synthetase knockdown cells. Toxicol In Vitro 2010;24:1032–8.
[33] Guengerich FP, MacDonald JS. Applying mechanisms of chemical toxicity to predict drug safety. Chem Res Toxicol 2007;20:344–69.
[34] Hosomi H, Fukami T, Iwamura A, Nakajima M, Yokoi T. Development of a highly sensitive cytotoxicity assay system for CYP3A4-mediated metabolic activation. Drug Metab Dispos 2011;39:1388–95.

Glycobiology vol. 23 no. 3 pp. 322–336, 2013
doi:10.1093/glycob/cws159
Advance Access publication on November 15, 2012

A novel antibody for human induced pluripotent stem cells and embryonic stem cells recognizes a type of keratan sulfate lacking oversulfated structures

Keiko Kawabe[2,3], Daiki Tateyama[3], Hidenao Toyoda[4], Nana Kawasaki[5], Noritaka Hashii[5], Hiromi Nakao[2], Shogo Matsumoto[2], Motohiro Nonaka[2,†], Hiroko Matsumura[3], Yoshinori Hirose[4], Ayaha Morita[4], Madoka Katayama[6], Makoto Sakuma[6], Nobuko Kawasaki[2], Miho Kusuda Furue[3], and Toshisuke Kawasaki[1,2]

[2]Research Center for Glycobiotechnology, Ritsumeikan University, Noji-Higashi, 1-1-1, Kusatsu, Shiga 525-8577, Japan; [3]Laboratory of Stem Cell Cultures, Department of Disease Bioresources, National Institute of Biomedical Innovation, Ibaraki, Osaka 567-0085, Japan; [4]Laboratory of Bio-analytical Chemistry, Faculty of Pharmaceutical Sciences, Ritsumeikan University, Shiga 525-8577, Japan; [5]Division of Biological Chemistry and Biologicals, National Institute of Health Sciences, Tokyo 158-8501, Japan; and [6]Biologicals Group, Research and Development Department, Seikagaku Biobusiness Corporation, Tokyo 207-0021, Japan

Received on August 19, 2012; revised on October 26, 2012; accepted on November 2, 2012

We have generated a monoclonal antibody (R-10G) specific to human induced pluripotent stem (hiPS)/embryonic stem (hES) cells by using hiPS cells (Tic) as an antigen, followed by differential screening of mouse hybridomas with hiPS and human embryonal carcinoma (hEC) cells. Upon western blotting with R-10G, hiPS/ES cell lysates gave a single but an unusually diffuse band at a position corresponding to >250 kDa. The antigen protein was isolated from the induced pluripotent stem (iPS) cell lysates with an affinity column of R-10G. The R-10G positive band was resistant to digestion with peptide *N*-glycanase F (PNGase F), neuraminidase, fucosidase, chondrotinase ABC and heparinase mix, but it disappeared almost completely on digestion with keratanase, keratanase II and endo-β-galactosidase, indicating that the R-10G epitope is a keratan sulfate. The carrier protein of the R-10G epitope was identified as podocalyxin by liquid chromatography/mass spectrometry (LC/MS/MS) analysis of the R-10G positive-protein band material obtained on sodium dodecyl sulfate–polyacrylamide gel electrophoresis (SDS-PAGE). The R-10G epitope is a type of keratan sulfate with some unique properties. (1) The epitope is expressed only on hiPS/ES cells, i.e. not on hEC cells, unlike those recognized by the conventional hiPS/ES marker antibodies. (2) The epitope is a type of keratan sulfate lacking oversulfated structures and is not immunologically cross-reactive with high-sulfated keratan sulfate. (3) The R-10G epitope is distributed heterogeneously on hiPS cells, suggesting that a single colony of undifferentiated hiPS cells consists of different cell subtypes. Thus, R-10G is a novel antibody recognizing hiPS/ES cells, and should be a new molecular probe for disclosing the roles of glycans on these cells.

Keywords: embryonic stem cells / induced pluripotent stem cells / keratan sulfate / monoclonal antibody / podocalyxin

Introduction

Carbohydrate-recognizing antibodies are extremely useful experimental tools for monitoring the changes in cell surface glycan structures as well as for identification of specific glycans on a specific cell type with high sensitivity and strict specificity. This is true in the case of pluripotent stem cells, including human embryonic stem (hES) and human-induced pluripotent stem (hiPS) cells (Wright and Andrews 2009). Among the conventional hiPS/ES cell-marker antibodies, stage-specific embryonic antigen (SSEA)-3 (Shevinsky et al. 1982) and SSEA-4 (Kannagi, Cochran et al. 1983; Kannagi, Levery et al. 1983) specifically recognize globosides such as Gal(β1-3)GalNAc(β1-3)Gal(α1-)-Cer and tumor rejection antigen (TRA)-1-60 (Andrews et al. 1984), TRA-1-81 (Andrews et al. 1984), germ cell tumor monoclonal (GCTM)2 (Pera et al. 1988; Cooper et al. 1992) and GCTM343 (Pera et al. 1988) recognize keratan sulfate (Adewumi et al. 2007). Keratan sulfate is a class of glycosaminoglycan (GAG). But in contrast to other GAGs, it does not contain uronic acids, and its repeating disaccharide unit is composed of alternating D-galactose (Gal) and *N*-acetyl-D-glucosamine (GlcNAc) residues. In most cases, the hydroxyl groups at the C-6 position of GlcNAc residues and/or Gal residues are sulfated. The keratan sulfate-glycan chains are linked to the polypeptide backbone through either *N*- or *O*-linkages, and are occasionally modified with sialic acid and fucose.

It should be kept in mind, however, that most of the above antibodies were generated against hEC cells: 2102Ep for

[1]To whom correspondence should be addressed: Tel: +81-77-3444; Fax: +81-77-3496; e-mail: tkawasak@fc.ritsumei.ac.jp
[†]A JSPS research fellow.

TRA-1-60, TRA-1-81 and SSEA-4 and GCT27 for GCTM2 and GCTM343. In other words, these antibodies are not specific to hiPS/ES cells; rather, they recognize those glycans that are common to hiPS/ES and embryonal carcinoma (EC) cells. ES cells and EC cells are very closely related cells and have many properties in common, but EC cells are teratocarcinoma. New antibodies that are capable of distinguishing between malignant and normal phenotype would be valuable. With this background, we tried to generate antibodies specific to hiPS cells. We first selected hiPS cell-positive hybridomas, from which hEC cell-positive hybridomas were excluded. By this procedure, we have obtained three antibodies that are capable of distinguishing between hiPS/ES and hEC cells. From these novel antibodies, we have chosen one, designated R-10G, and the biochemical properties of the antibody and its epitope molecules have been investigated. The results demonstrated clearly that R-10G is a novel marker antibody recognizing a type of keratan sulfate lacking oversulfated structures on hiPS cells, and thus should be useful not only as a new molecular probe for disclosing the roles of glycans on the surface of hiPS cells in the maintenance of self-renewal and pluripotency and during the process of differentiation, but also as a potent tool for the evaluation and standardization of hiPS cells with different tissue origins and different histories in regenerative medicine.

Results

Generation of monoclonal antibodies to hiPS cells

In order to raise a panel of monoclonal antibodies to cell surface markers on hiPS cells, freeze-thawed Tic cells in phosphate-buffered saline (PBS) were mixed with Freund's complete adjuvant (FCA) and used to immunize C57BL/6 mice intraperitoneally or subcutaneously. Primary screening of a total of 960 hybridomas using Tic cell-fixed plates and MRC-5 cell-fixed plates (controls) indicated that 29 hybridomas produced antibodies that exhibited reactivity to surface antigens on Tic cells. Secondary screening was performed for these hybridomas to determine the reactivities of the antibodies to a hEC cell line, 2102Ep and mouse embryonic fibroblast (MEF).

As shown in Table I, a large portion of the antibody panel (Nos. 2, 4, 6, 9, 13, 19, 20, 21, 25, 26, 27, 28 and 29) exhibited significant binding activity not only to Tic cells but also to 2102Ep cells, an EC cell line. Interestingly, however, antibody Nos. 10, 11 and 17 exhibited strong reactivity toward Tic cells but no or very weak reactivity toward 2102Ep cells. These results demonstrated clearly that there are definite differences in the antigen profiles between hiPS and hEC cells, even though there is considerable overlapping between them. The binding of these antibodies to human iPS cells was confirmed by western blotting, in which Tic cell lysates were resolved by sodium dodecyl sulfate–polyacrylamide gel electrophoresis (SDS–PAGE) and the culture supernatants of hybridomas were used as primary antibodies. The protein profiles of SDS–PAGE and some representative western blot profiles of Tic cell lysates (7/29 hybridomas) are presented in Figure 1A and B, respectively.

Tic cell lysates gave a large number of protein bands corresponding to from 15 to >300 kDa. On the other hand, the migration positions and the intensities of the immunoreactive bands were characteristic of the respective hybridomas, but these bands appear to be classifiable into three groups on the basis of their apparent molecular sizes: Between 35 and 50 kDa (e.g. clone 27), between 75 and 100 kDa (e.g. clone 25) and over 250 kDa (e.g. clones 10 and 26). Such antibodies that show strong binding in the cell plate assay but a faint or essentially no band on western blotting might interact with

Table I. Summary of hybridoma screening by cell plate binding assaying

No.	Tic	2102Ep	MRC-5	MEF	No.	Tic	2102Ep	MRC-5	MEF
1	++	+++	±	−	16	+	+	±	±
2	+++	++	+	−	17	++++	±	−	−
3	+	+	−	−	18	++	++	−	−
4	+++	++	−	−	19	+++	+++	−	−
5	++	±	−	−	20	+++	+++	++	±
6	+++	+++	+	−	21	+++	+++	+	±
7	++	++	±	−	22	++	++	−	−
8	+	+++	+	−	23	++	++	++	−
9	+++	+++	−	−	24	+	+	−	−
10	+++	±	−	−	25	++	+++	+	±
11	+++	+	−	−	26	++++	+++	−	−
12	+	++++	−	−	27	+++	+++	+	−
13	+++	+++	±	±	28	+++	+++	−	−
14	++	+	−	−	29	+++	+++	−	−
15	+	++	−	−					

The culture supernatant of each hybridoma was added to cell-fixed screening plates (Tic, 2102Ep, MRC-5 and MEF cells), and binding of antibodies to the cells was monitored by DAB staining under a light microscope after treatment with HRP-conjugated anti-mouse IgG as described under Materials and methods. The results are presented as a 5-grade scale from − to ++++.

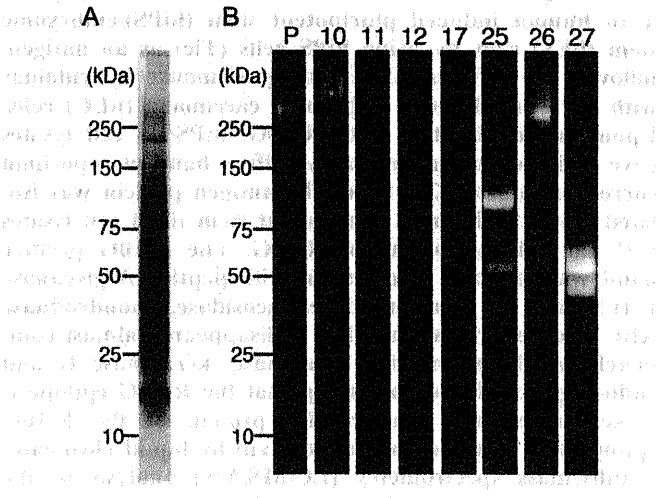

Fig. 1. Screening of hybridomas by western blotting. Tic cell lysates in the complete RIPA buffer (15 μg protein) were resolved by SDS–PAGE on a 4–15% gradient gel under nonreducing conditions, followed by immunoblot detection with antibodies secreted into the medium from the respective hybridomas as described under Materials and methods. (**A**) Gel code blue staining of SDS–PAGE of the Tic cell lysates. (**B**) Western blotting. The numbers at the top of each column indicate the clone number of hybridomas. P: Antibody TRA-1-60 (positive control). The molecular mass markers are shown on the left.

membrane lipid components (e.g. clones 11, 12 and 17). In lane P, TRA-1-60, a conventional iPS/ES marker antibody, which was used as a positive control, gave a single but a diffuse band in the high-molecular-weight region over 250 kDa, as was expected from a previous report (Andrews et al. 1984). The results of the cell-binding assay indicated that three hybridomas Nos. 10, 11 and 17 seemed to be appropriate to pursue our aim. Of these hybridomas, we focused on No. 10, since these hybridomas exhibited a most striking band upon western blotting as shown in Figure 1B. The hybridoma R-10G was a subclone obtained from hybridoma No. 10. The isotype of antibody R-10G is IgG1.

Binding properties of R-10G as to iPS/ES/EC cells

We examined the binding activity of R-10G toward some other hiPS/ES/EC cell lines using an InCell analyzer 2000 in comparison with those of conventional hiPS and mouse iPS/ES marker antibodies, TRA-1-81, TRA-1-60, SSEA-1, SSEA-3 and SSEA-4. The results of immunocytochemical studies are summarized in Figure 2 (A–F). As shown in (A), antibody R-10G interacted remarkably with three different hiPS cell lines: Tic cells (68 ± 7%, mean percentage binding in four experiments ± SD), 201B7 cells (88 ± 7%) and Squeaky cells (79 ± 9%), and also with two hES cell lines: H9 cells (64 ± 4%) and KhES-3 cells (83 ± 2%). TRA-1-81 (B), TRA-1-60 (C), SSEA-3 (D) and SSEA-4 (E) also exhibited high binding activities of 96–99, 94–99, 64–72 and 85–99%, toward these five types of hiPS/ES cells, respectively, all being consistent with previous studies (Wright and Andrews 2009). These results indicated that R-10G is a hiPS/ES-recognizing antibody like the other conventionally used hiPS/ES marker antibodies. Most importantly, however, in contrast to the other conventional iPS/ES marker antibodies, which bound to an EC cell line, 2102Ep, as effectively as to other iPS/ES cells (68–98%), R-10G did not bind to an EC cell line, 2102Ep, significantly (6 ± 1%) (A). This was confirmed by essentially no binding of R-10G to a different EC cell line, NCR-G3 (data not shown). Taken together, these results indicated clearly that R-10G is a unique iPS/ES marker antibody, which distinguishes between hiPS and hEC cells. SSEA-1 (in F), which is known to be negative as to undifferentiated hiPS/ES/EC cells (Wright and Andrews 2009) did not show significant binding to any of the cell lines used in this experiment, as expected.

Then, we examined the localization of these epitopes on the surface of hiPS (Tic) cells by means of immunocytochemical experiments using a laser confocal scanning microscope. As shown in Figure 3 (A and B), at a low magnification (×100), almost all the TO-PRO 3 (nuclear counterstained)-positive cells in a colony appeared to be stained with R-10G in green, although there were significant differences at the level of staining depending upon the cells. TRA-1-81 appeared to stain also almost all cells ubiquitously in red. However, when the two images were merged into a single one, it was found that the cells in the central region of the colony were largely stained in green, while those in the peripheral region were largely stained in red. This apparent polarity of the epitope expression may be

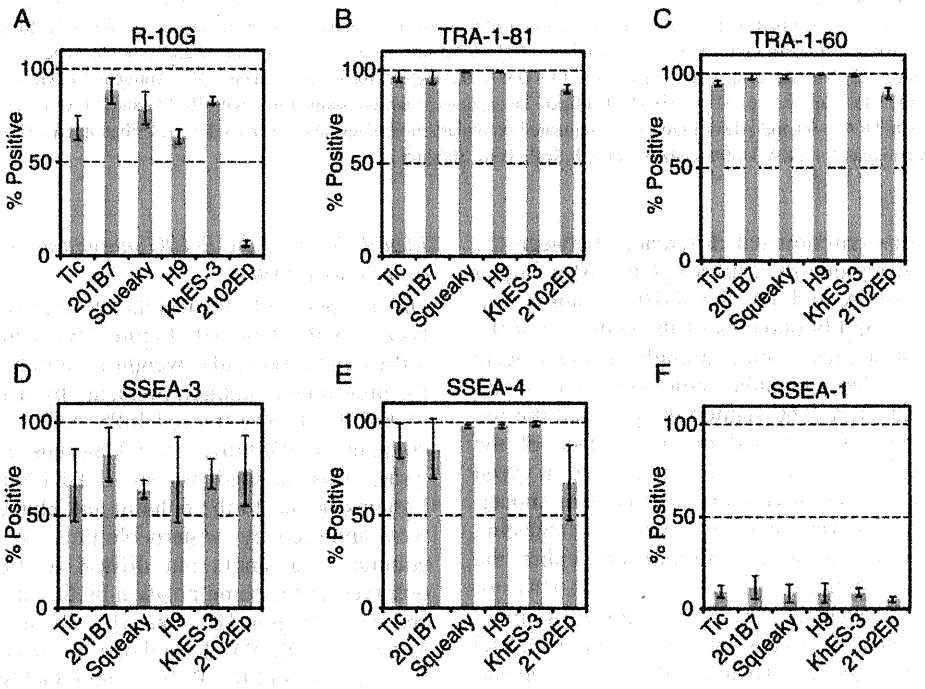

Fig. 2. Characterization of R-10G as an iPS/ES marker antibody using an InCell Analyzer. HiPS cells (Tic, 201B7, and Squeaky), hES cells (H9 and KhES-3) and hEC cells (2102Ep) seeded onto 24-well plates were fixed in 4% PFA and then incubated with monoclonal antibodies (R-10G, TRA-1-81, TRA-1-60, SSEA-3, SSEA-4 and SSEA-1) at 4°C overnight. Binding of antibodies to the cells was visualized by incubation with Alexa Fluor 647-conjugated chicken anti-mouse IgG and then quantitated using an InCell Analyzer 2000 and Developer Toolbox ver1.8 as described under Materials and methods. Error bars represent standard deviation from the mean ($n = 4$).

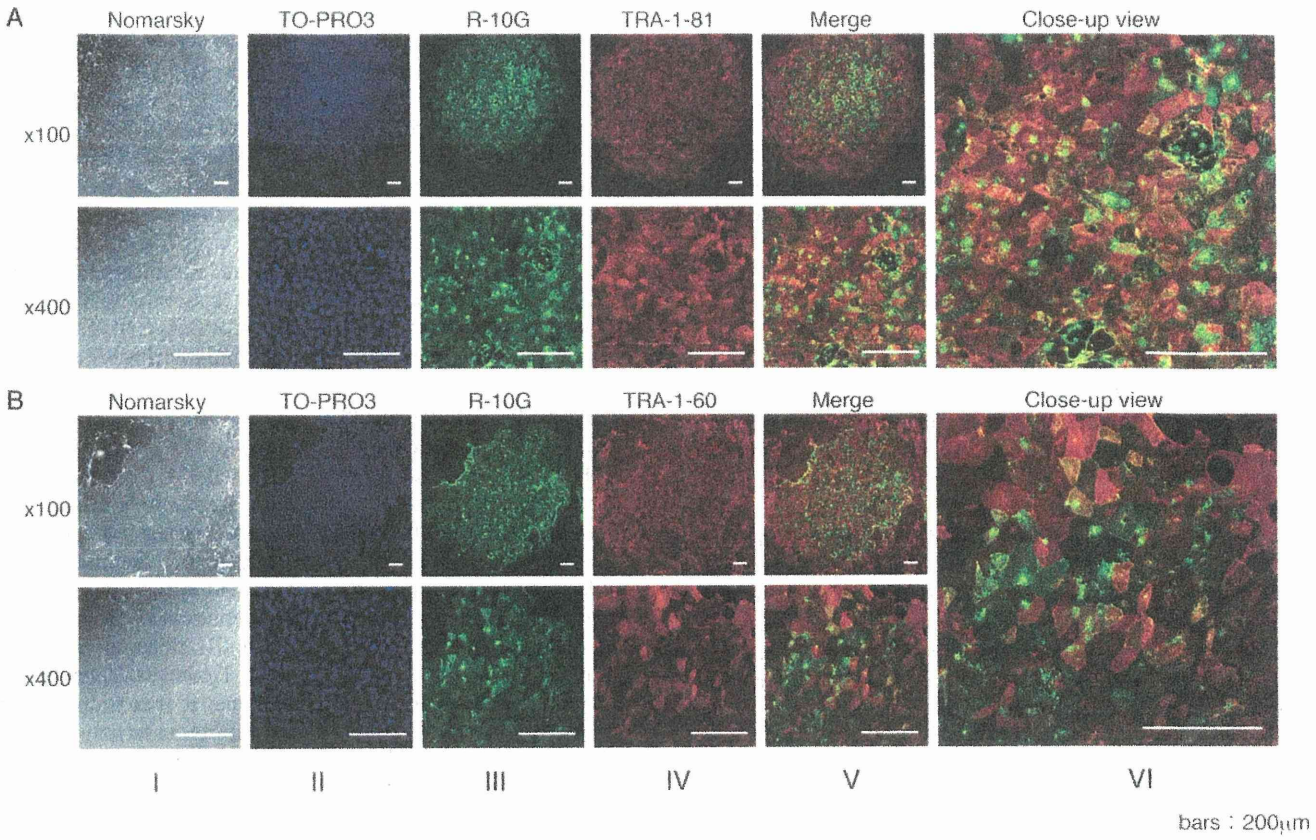

Fig. 3. Localization of the R-10G, TRA-1-81 and TRA-1-60 epitopes on cultured Tic cells visualized on laser confocal microscopy. (**A**) Tic cells cultured on Millipore EZ slides were double-stained first with R-10G and Alexa Fluor 488-conjugated secondary (anti-mouse IgG1) antibody, followed by with TRA-1-81 and Alexa Fluor 555-conjugated secondary (anti-mouse IgM) antibody. Cells were observed at two different magnifications: ×100 (upper panel) and ×400 (lower panel). (I) Nomarski imaging. (II) Nuclear counterstaining with TO-PRO3. (III) Antigens for R-10G (green). (IV) Antigens for TRA-1-81 (red). (V) Merged image of (III) and (IV). (VI) Close-up view of V (×400). (**B**) Cultured Tic cells were double-stained first with R-10G and Alexa Fluor 488-conjugated secondary antibodies, followed by with TRA-1-60 and Alexa Fluor 555-conjugated secondary antibodies, and visualized as described in (**A**). (I)–(IV) are the same as in (**A**) except for (IV), in which antigens for TRA-1-60 are shown in red. Scale bars, 200 μm.

related to some micro-environmental differences between the central and peripheral regions of a hiPS colony. At a higher magnification (×400, in A and B), the R-10G staining was detected on the surface and boundaries of the cells, but at the same time granular structures stained strongly in green were found in the cytosol. These granular structures were hardly seen in TRA-1-81 and TRA-1-60 stained images, and the red staining was predominantly detected on the surface of the cells. In merged images, some Tic cells were stained in green and the other cells in red, although there were cells or subcellular regions of cells that were stained in yellow, suggesting that some of the cells expressed predominantly either the R-10G or TRA-1-81 epitope, or either the R-10G or TRA-1-60 epitope. However, there were a significant number of cells that co-expressed these two pairs of epitopes (R-10G and TRA-1-81 epitopes and R-10G and TRA-1-60 epitopes) in comparable ratios in close vicinity. These results suggested that hiPS cells are in fact heterogeneous with regard to the expression of cell surface glycans from cell to cell, and suggested the presence of subtypes of cells within a single colony of hiPS cells.

Identification of the R-10G antigen molecule as a podocalyxin

On the basis of the results of western blotting of Tic cell lysates with clone 10 (Figure 1B), which gave a single but diffuse high-molecular-weight protein band, we tried to isolate the presumptive antigen molecule by using an affinity column of R-10G. Freeze-thawed hiPS cells were solubilized in the complete RIPA buffer (see Materials and methods), and the lysate was applied to an R-10G-Sepharose 4B column. Proteins bound to the column and eluted with pH 11.5 buffer were analyzed by western blotting. As shown in Figure 4A, column 1, a single but diffuse R-10G positive band was observed at the same position as that in the case of the whole cell lysate (Figure 1B, clone 10). The isolated antigen was subjected to SDS–PAGE and the resolved protein bands were stained with SYPRO Ruby Protein Gel Stain. The bands corresponding to those on western blotting were excised as three fractions (a, b and c in column 2), and then subjected to *in-gel* trypsin digestion, and the peptides released were analyzed by LC/MS/MS. The three fractions of the major western blotting band generated several peptides sequences, all of which

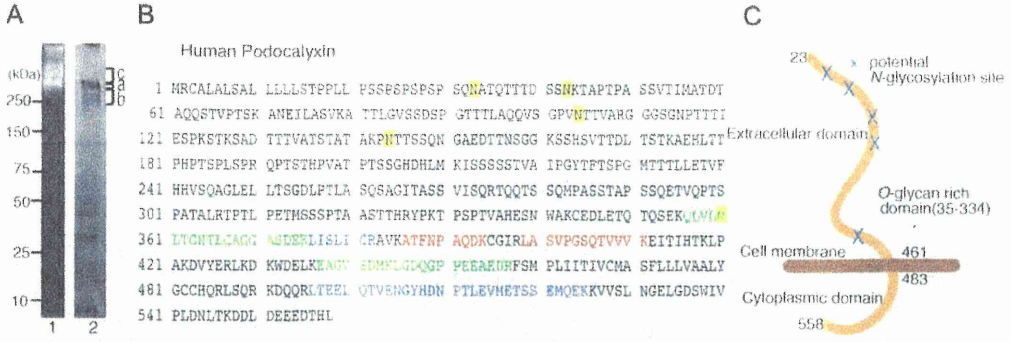

Fig. 4. Isolation and identification of the antigen protein carrying the R-10G epitope. **(A)** R-10G antigen proteins isolated from Tic cell lysates with an R-10G-affinity column were resolved by SDS–PAGE on a 4–15% gradient gel under nonreducing conditions. The resolved proteins were transferred to a PVDF membrane, followed by immunoblot detection with R-10G (column 1, the isolated antigens derived from 5×10^4 cells). The molecular mass markers are shown on the left. The gel was stained with SYPRO Ruby Protein Gel Stain (column 2, the isolated antigens derived from 3.5×10^5 cells), and the protein bands, a, b and c, i.e. the middle/major, higher and lower molecular size immunoblot bands, were excised from the gel. After *in-gel* trypsin digestion, the peptides released from the gel were subjected to LC/MS/MS analysis as described under Materials and methods. **(B)** Identification of the R-10G antigen protein by MS. The identified peptides in bands a, b and c are shown in red letters, those in bands a and b in blue and those in band b in green within the complete human podocalyxin sequence. The potential *N*-glycosylation sites (33, 43, 104, 144 and 360) are indicated by yellow-shaded areas. **(C)** Schematic representation of the membrane topology of human podocalyxin.

corresponded to partial sequences of human podocalyxin (Figure 4B), and no other alternative sequence was detected for these fractions *a*, *b* and *c*.

Podocalyxin is a heavily glycosylated type-1 transmembrane protein belonging to the CD34 family of sialomucins (Sassetti et al. 1998, 2000) (Figure 4C). The protein was originally described as the major sialoprotein on podocytes of the kidney glomerulus (Kerjaschki et al. 1984). Recently, podocalyxin was shown to be expressed by hematopoietic progenitors, vascular endothelia and a subset of neurons, and it is aberrantly expressed in a number of tumors (Nielsen and McNagny 2009). The human podocalyxin gene (Kershaw, Wiggins et al. 1997) encodes a protein of 558 amino acids. Because the extracellular domain of podocalyxin is extensively glycosylated with sialylated *O*-linked carbohydrates and five potential *N*-linked glycosylation sites, the approximate molecular weight of podocalyxin is 160–165 kDa (Kershaw, Beck et al. 1997). Interestingly, podocalyxin was identified to be highly expressed in undifferentiated hES cells (Brandenberger et al. 2004; Cai et al. 2006). In addition, the TRA-1-81 and TRA-1-60 epitopes have been shown to be expressed on a 200 kDa form of podocalyxin (Schopperle and DeWolf 2007). Identification of podocalyxin as the R-10G antigen protein constituted evidence that podocalyxin polypeptide serves as a common carrier for a family of epitopes generated through carbohydrate modifications on the human pluripotent cell surface.

Characterization of the R-10G epitope by glycosidase digestion and western blotting

The unusual diffuse shape of the R-10G reactive band (Figure 1B, clone 10 and Figure 4A) suggested that the band is most probably of a glycoprotein. To examine this, we digested a Tic cell lysate and/or R-10G antigen isolated therefrom with various glycosidases prior to SDS–PAGE, and determined the effects of these treatments on the intensities and the migration positions of the R-10G reactive bands. This experiment was carried out with two other hiPS/ES marker antibodies, TRA-1-81 and TRA-1-60, which have been shown to recognize keratan sulfate (Adewumi et al. 2007) and sialylated keratan sulfate (Badcock et al. 1999), respectively.

As shown in Figure 5A (lanes 1, 3 and 5), upon western blotting, Tic cell lysates gave diffuse bands not only with R-10G but also with TRA-1-81 and TRA-1-60 in high-molecular-weight regions (>250 kDa), this being consistent with the potent immunocytochemical activities of these antibodies toward Tic cells, as described above. Then, we examined the reactivity of the isolated R-10G antigen toward R-10G, TRA-1-81 and TRA-1-60 (Figure 5A, lanes 2, 4 and 6). Unexpectedly, the isolated R-10G antigen reacted not only with R-10G but also with TRA-1-81 and TRA-1-60, giving a single band at the respective positions expected from those for the Tic cell lysates. These results suggested that these three antibodies recognize similar glycans in the same category, keratan sulfate, as their epitopes. In agreement with this hypothesis, upon digestion of the R-10G antigen with keratanase II, which degrades keratan sulfate specifically (see Figure 6), the R-10G epitope as well as the TRA-1-81 epitope was degraded (Figure 5B). It should be noted, however, that the most of the R-10G epitope disappeared easily with a small amount of the enzyme, whereas the TRA-1-81 epitope was relatively stable as to the digestion and was degraded only when a large amount of the enzyme was added. These results suggested that R-10G and TRA-1-81 share a common epitope, keratan sulfate, although the epitope structures recognized by these antibodies are different from each other in some unspecified way.

Following this initial experiment involving keratanase II, we studied the properties of the R-10G epitope by the same means with various GAG-degrading enzymes. As shown in Figure 5C, chondroitinase ABC, which degrades essentially all the chondroitin sulfate subfamily, and the heparinase mix, a mixture of heparinase, heparitinase I and heparitinase II,

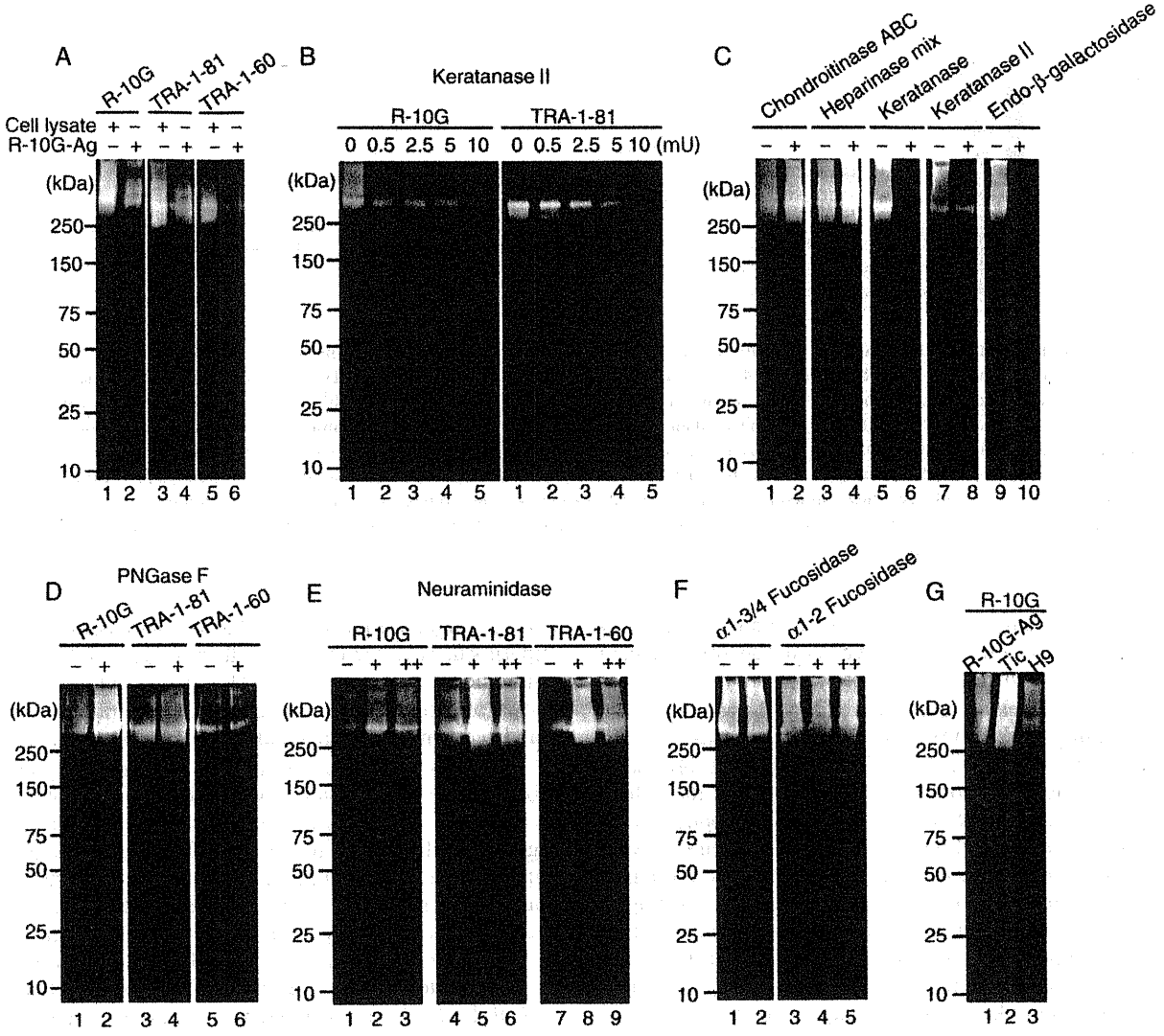

Fig. 5. Characterization of the R-10G epitope by glycosidase digestion and western blotting. Tic cell lysates (12 μg protein, corresponding to 1×10^5 cells) and/or the isolated R-10G antigen (corresponding to $\sim 1 \times 10^5$ cells), which had been incubated with and without predigestions with various glycosidases, were subjected to SDS–PAGE on a 4–15% gradient SDS-polyacrylamide gel under nonreducing conditions except for PNGase F digestion, followed by western blotting with R-10G and other undifferentiated cell-marker antibodies as described under Materials and methods. (**A**) Western blotting of Tic cell lysates and the R-10G antigen with R-10G, TRA-1-81 and TRA-1-60. (**B**) The R-10G antigen was digested with increasing amounts of keratanase II and the digests were analyzed by western blotting with R-10G and TRA-1-81. (**C**) The R-10G antigen was digested with chondroitinase ABC (lane 2), heparinase mix (lane 4), keratanase (lane 6), keratanase II (lane 8) or endo-β-galactosidase (lane 10) and the digests were analyzed by western blotting with R-10G. Lanes 1, 3, 5, 7 and 9: No enzyme added. (**D**) The R-10G antigen was digested with PNGase F, and the digests were analyzed by western blotting with R-10G (lane 2), TRA-1-81 (lane 4) and TRA-1-60 (lane 6). Lanes 1, 3 and 5: No enzyme added. (**E**) The R-10G antigen was digested with neuraminidase from *Arthrobacter ureafaciens* of 3.75 mU (lanes 2, 5 and 8) or 37.5 mU (lanes 3, 6 and 9) and the digests were analyzed by western blotting with R-10G (lanes 1, 2 and 3), TRA-1-81 (lanes 4, 5 and 6) and TRA-1-60 (lanes 7, 8 and 9). Lanes 1, 4 and 7: No enzyme added. (**F**) The R-10G antigen was digested with α1–3/4 fucosidase (lane 2: 15 μU) or α1–2 fucosidase (lanes 4 and 5: 0.33 and 2.0 U, respectively), and the digests were analyzed by western blotting with R-10G. Lanes 1 and 3: No enzyme added. (**G**) The R-10G antigens (lane 1), Tic cell lysates (15 μg protein, lane 2) and H9 cell lysates (15 μg protein, lane 3) were analyzed by western blotting with R-10G. The molecular mass markers are shown on the left of the respective panels, **A**–**G**.

which degrades various subtypes of heparan sulfates and heparins, did not decrease the R-10G binding activity; rather, the reactivity was enhanced to some extent for some undetermined reasons. These results indicated that neither heparan sulfate/heparin nor chondroitin sulfates are associated with the epitope structure as major constituents. On the other hand, keratanase and endo-β-galactosidase, both of which are keratan sulfate-degrading enzymes, abolished the R-10G binding activity as keratanase II did, confirming that the major epitope of R-10G is a keratan sulfate (see Figure 6).

Then, we studied the effect of PNGase F treatment. As shown in Figure 5D, PNGase F digestion of the R-10G antigen resulted in no decrease in the R-10G binding activity or the migration position of the major reactive band,

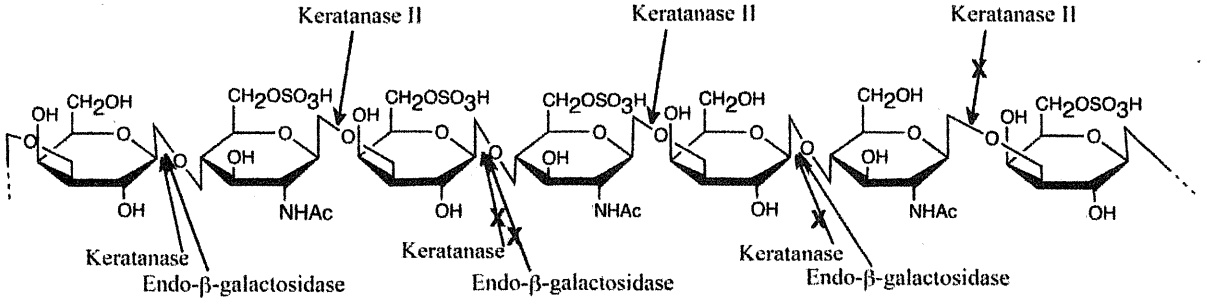

Fig. 6. Structural requirements of keratan sulfate-degrading enzymes. Schematic presentation of the specificities of keratanase II, keratanase and endo-β-galactosidase with regard to the effect of sulfate modification of the structural repeating units of keratan sulfate. The arrows marked with X indicate that the enzyme does not work.

indicating that *N*-linked glycans are not the major constituents of the epitope on the antigen. The same results were obtained for TRA-1-81 and TRA-1-60, excluding the major role of *N*-glycans as the epitope constituents.

The isolated R-10G antigen contained significant amounts of sialic acid and fucose (see Discussion). Since it was reported previously that the TRA-1-60 epitope was sialylated keratan sulfate, which was destroyed on digestion with neuraminidase either from *Vibrio cholerae* or from *Arthrobacter ureafaciens* (Andrews et al. 1991; Badcock et al. 1999). We examined the effects of these two neuraminidases on the immunoreactivity of the R-10G antigen by western blotting. As shown in Figure 5E, digestion of the R-10G antigen with neuraminidase from *Arthrobacter ureafaciens* resulted in no significant change in the immunoreactive bands for R-10G (lanes 1–3). The same results were obtained for the R-10G antigen with neuraminidase from *Vibrio cholerae* (data not shown). These results indicated that sialic acids are not associated with the R-10G epitope as a major constituent. Similarly, the reactivities of TRA-1-81 and TRA-1-60 to the R-10G antigen were not diminished upon digestion with neuraminidase from *Arthrobacter ureafaciens* (lanes 4–9). Instead, their reactivities were enhanced (lane 4 vs. lanes 5, 6, lane 7 vs. lanes 8, 9), suggesting that sialylation blocks or sterically hinders these epitopes. The same results were obtained with neuraminidase from *Vibrio cholerae* (data not shown).

Recently, the Fuc(α1-2)Gal(β1-3)GlcNAc structure has been reported to be a pluripotency-associated epitope for SSEA-5, a newly established hES marker monoclonal antibody (Tang et al. 2011), and for BC2LCN, a lectin isolated from a Gram-negative bacterium *Burkholderia cenocepacia* (Sulak et al. 2010; Tateno et al. 2011). Then, we studied the effects of α-fucosidase treatment on the immunoreactivity of the R-10G antigen. As shown in Figure 5F, digestion of the R-10G antigen neither with α1-3/4 fucosidase nor with α1-2 fucosidase indicated any detectable changes on the immunoreactive bands, excluding the major roles of fucose residue as the R-10G epitope constituents and exhibiting the differences in binding specificity between R-10G and SSEA-5 or BC2LCN.

Figure 5G demonstrated that the R-10G epitope was expressed also on hES cells. Upon western blotting, an H9 cell extract, prepared by the same procedure as described above for Tic (hiPS) cells under Materials and methods, gave an R-10G positive band almost at the same position as for the iPS (Tic) cell lysates and also for the R-10G antigen isolated therefrom. These results are consistent with those of image analysis (Figure 2), in which R-10G bound to two hES cell lines, H9 and KhES-3, as effectively as to iPS cell lines, Tic, 2101B7 and Squeaky, like most of the conventional hiPS/ES marker antibodies.

Further characterization of the R-10G epitope by chemical analysis

In the next experiment, the oligosaccharides released from the R-10G antigen with keratan sulfate-degrading enzymes were analyzed by reverse-phase ion-pair HPLC system using a fluorometric post-column detection method newly developed by Hirose et al (in preparation). Figure 7A shows the oligosaccharide profiles released with keratanase II, which hydrolyzes the 1,3-β-glucosaminidic linkages to galactose in keratan sulfate, when the 6-O-position of GalNAc is sulfated (Brown et al. 1995; Oguma et al. 2001) (see Figure 6). A predominant peak was detected at 6.60 min, which corresponds to the disaccharide-repeating units of keratan sulfate, Gal-GlcNAc (6S) (peak 1), followed by a small peak corresponds to Gal-GlcNAc(6S)-Gal-GlcNAc(6S) (peak 2) and some very minor peaks, which include a negligible peak at the position corresponded to Gal(6S)-GlcNAc(6S) (peak 3). The sulfation index of the GAG family, the average number of sulfate residues per disaccharide-repeating unit, Gal-GlcNAc, was calculated to be 1.02. Figure 7B shows the oligosaccharide profiles released with endo-β-galactosidase, which hydrolyzes the 1,4-β-galactosidic linkage when the 6-O-position of the Gal residue is not sulfated, irrespective of the presence or absence of sulfate on the adjacent GalNAc (Fukuda and Matsumura 1976). One major peak was detected at 6.36 min, which corresponds to the disaccharide-repeating units of keratan sulfate, GlcNAc(6S)-Gal (peak 5), followed by several significant peaks between peak 5 and peak 6. Figure 7C shows the elution profile of endo-β-galactosidase digests of the keratan sulfate from bovine cornea, which was used as a standard of keratan sulfate. Three major peaks such as peaks 5, 6 and 7 were obtained, which correspond to GlcNAc(6S)-Gal, GlcNAc (6S)-Gal(6S)-GlcNAc(6S)-Gal and GlcNAc(6S)-Gal (6S)-GlcNAc(6S)-Gal(6S)-GlcNAc(6S)-Gal, respectively. The presence of peaks 6 and 7 in Figure 7C but no or little peaks at the corresponding positions in Figure 7B may be explained by